AD-A033 218 IOWA UNIV IOWA CITY DEPT OF PHYSICS AND ASTRONOMY F/G 4/1
THE ANGULAR DISTRIBUTION OF AURORAL KILOMETRIC RADIATION.(U)
AUG 76 J L GREEN, D A GURNETT, S D SHAWHAN N00014-76-C-0016
UNCLASSIFIED U. OF IOWA-76-28 NL

| OF |
AD A033218

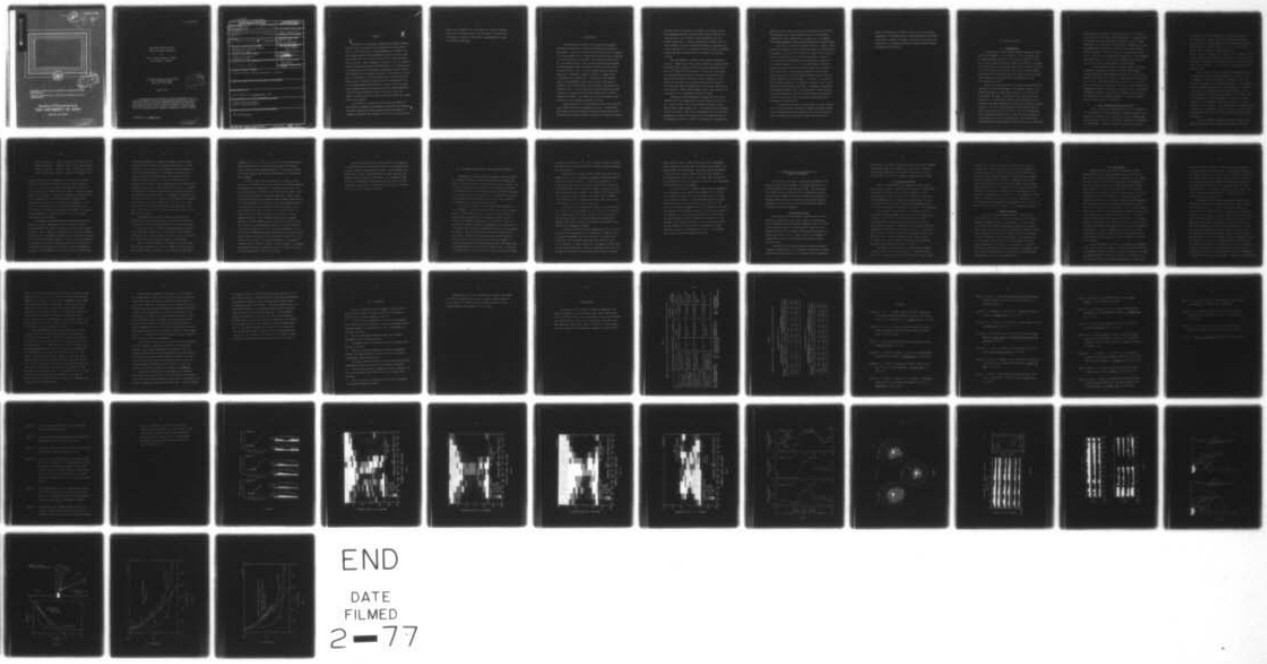

END

DATE FILMED
2-77

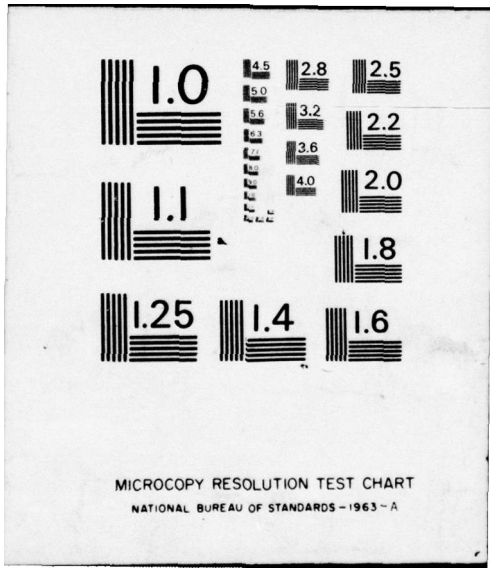
1.0
1.1
1.25
1.4
1.6
1.8
2.0
2.2
2.5
2.8
3.2
3.6
4.0
4.5
5.0
5.6
6.3
MICROCOPY RESOLUTION TEST CHART
NATIONAL BUREAU OF STANDARDS - 1963 - A

U. of Iowa 76-28

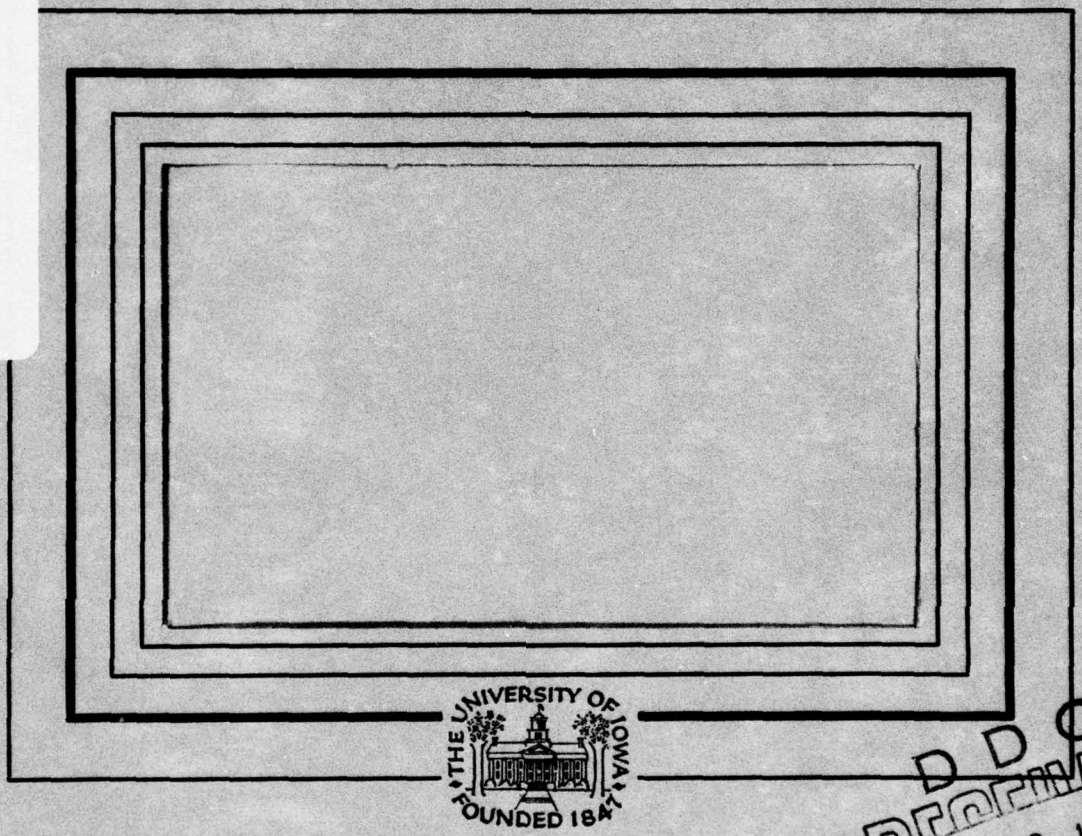

"Research was supported in part by the Office of Naval Research under contract N00014-76-C-0016."

Department of Physics and Astronomy

THE UNIVERSITY OF IOWA

Iowa City, Iowa 52242

U. of Iowa 76-28

The Angular Distribution of Auroral Kilometric Radiation[+]

by

James L. Green, Donald A. Gurnett
and Stanley D. Shawhan

Department of Physics and Astronomy
The University of Iowa
Iowa City, Iowa 52242

August, 1976

The research at the University of Iowa was supported by the National Aeronautics and Space Administration through Grants NGL-16-001-002 and NGL-16-001-043; through Contracts NAS1-11257 and NAS1-13129 with Langley Research Center, and through Contracts NAS5-11074, and NAS5-11431 with Goddard Space Center; by the Office of Naval Research, and by the National Science Foundation, Atmospheric Sciences Section.

[+]Submitted to J. Geophys. Res.

UNCLASSIFIED

SECURITY CLASSIFICATION OF THIS PAGE (When Data Entered)

REPORT DOCUMENTATION PAGE

READ INSTRUCTIONS BEFORE COMPLETING FORM

1. REPORT NUMBER: U. of Iowa-76-28	2. GOVT ACCESSION NO.
3. RECIPIENT'S CATALOG NUMBER	
4. TITLE (and Subtitle): THE ANGULAR DISTRIBUTION OF AURORAL KILOMETRIC RADIATION,	5. TYPE OF REPORT & PERIOD COVERED: Progress December 1973
	6. PERFORMING ORG. REPORT NUMBER
7. AUTHOR(s): J. L. Green, D. A. Gurnett and S. D. Shawhan	8. CONTRACT OR GRANT NUMBER(s): N00014-76-C-0016; NGL-16-001-002
9. PERFORMING ORGANIZATION NAME AND ADDRESS: Department of Physics and Astronomy, The University of Iowa, Iowa City, IA 52242	10. PROGRAM ELEMENT, PROJECT, TASK AREA & WORK UNIT NUMBERS: 59p.
11. CONTROLLING OFFICE NAME AND ADDRESS: Office of Naval Research, Arlington, VA 22217	12. REPORT DATE: August 1976
	13. NUMBER OF PAGES: 57
14. MONITORING AGENCY NAME & ADDRESS (if different from Controlling Office): Progress rept.	15. SECURITY CLASS. (of this report): UNCLASSIFIED
	15a. DECLASSIFICATION/DOWNGRADING SCHEDULE

16. DISTRIBUTION STATEMENT (of this Report)

Approved for public release; distribution is unlimited.

17. DISTRIBUTION STATEMENT (of the abstract entered in Block 20, if different from Report)

18. SUPPLEMENTARY NOTES

To be published in J. Geophys. Res., 1976.

19. KEY WORDS (Continue on reverse side if necessary and identify by block number)

Auroral kilometric radiation
electric field measurements

20. ABSTRACT (Continue on reverse side if necessary and identify by block number)

[See page following.]

DD FORM 1 JAN 73 1473 EDITION OF 1 NOV 65 IS OBSOLETE S/N 0102-014-6601

UNCLASSIFIED 188 460

SECURITY CLASSIFICATION OF THIS PAGE (When Data Entered)

ABSTRACT

Measurements of the angular distribution of auroral kilometric radiation (AKR) are presented using observations from the Hawkeye 1, IMP 6, and IMP 8 satellites. The wave experiments on Hawkeye 1 and IMP 6 provide electric field measurements of AKR in narrow frequency bands centered at 178, 100, and 56.2 kHz and IMP 8 provides measurements at 500 kHz. From a frequency of occurrence survey, at satellite radial distances greater than 7 R_e (earth radii), it is shown that AKR is preferentially and instantaneously being beamed into solid angles of approximately 3.5 steradians at 178 kHz, 1.8 steradians at 100 kHz, and 1.1 steradians at 56.2 kHz, directed upward from the night time auroral zones. Simultaneous multiple satellite observations of AKR in the northern hemisphere show that the radiation occurs simultaneously throughout these solid angles and that the topside plasmapause acts as an abrupt propagation cutoff on the night side of the earth. On the day side of the earth this abrupt cutoff at the plasmapause is not observed.

The results of a computer ray tracing model qualitatively describing the propagation characteristics of AKR are also discussed. This model assumes small source locations emitting radiation at different frequencies from altitudes of 1.5 to 3.5 R_e in the auroral

zone at 24 hour magnetic local time along a 70° invariant latitude field line. The source locations closely satisfy the relation that the radiation is emitted at frequencies of approximately 3/2 times the electron gyrofrequency.

I. INTRODUCTION

Recent satellite observations have revealed two distinctly different non-thermal radio emissions associated with the earth's magnetosphere. Both types of emissions occur at kilometric wavelengths in the radio spectrum. One of these types of radiation has a relatively constant intensity and is very weak. The radiation has been called the 'non-thermal continuum' and is generated between the plasmapause and the magnetopause with the greatest intensity on the day side of the earth [Gurnett, 1975]. The other type of radiation, which has been called 'terrestrial kilometric radiation' by Gurnett [1974] and by Kaiser and Alexander [1976], consists of intense sporadic bursts of electromagnetic energy generated over a wide range of distances (2 to 15 earth radii) above the auroral zones [Kaiser and Alexander, 1976]. To avoid confusion with the non-thermal continuum radiation, Kurth et al. [1975] term this sporadic noise 'auroral kilometric radiation'. The present study considers satellite observations of auroral kilometric radiation (AKR) only.

Dunckel et al. [1970] first showed that AKR was correlated with large values of the auroral electrojet index (A_E). Gurnett [1974] also reported that during periods of magnetic substorm activity IMP 6 observed intense auroral kilometric radiation and as magnetic activity

decreased so did the frequency of occurrence and intensity of AKR. Using photographs produced from the optical scanner aboard the DAPP satellite Gurnett [1974] showed a close association of AKR with discrete auroral arcs. Ackerson and Frank [1972] observed that intense 'inverted V' electron precipitation events are correlated with discrete auroral arcs. The combination of these two lines of evidence suggests that AKR is associated with the inverted V precipitating electrons.

The power spectrum of AKR has a large degree of variability with time. Gurnett [1974] shows a power spectrum of a typical auroral kilometric burst as observed by IMP 8 that has a peak power flux of about 10^{-14} watts m^{-2} Hz^{-1} at 178 kHz. On either side of the peak the spectrum decreases rapidly in intensity to the receiver noise level at about 30 kHz and to near the cosmic background at 2 MHz. Kaiser and Stone [1975] show a power spectrum with peak frequency near 500 kHz and they also indicate that the peak may sometimes be as low as 130 kHz. Gurnett [1974] estimated that at peak intensity, the total power of AKR is sometimes as high as 10^9 watts.

Preliminary evidence presented by Gurnett [1974] at 178 kHz indicated that AKR is generated at radial distances as low as 2.8 R_e (R_e = earth's radius) in the evening auroral zone, from a source that "subtends a small angular size". The rotating electric antennas on IMP 8 and Hawkeye 1 were used by Kurth et al. [1975] to locate the average source region of AKR projected onto the equatorial plane at the frequency of 178 kHz. From IMP 8 observations the average source

region was found to be at a local time of 21.25 hours and at 0.835 R_e from the polar axis. Along an auroral field line (70° invariant latitude) this source region would be at about 2 R_e. The Hawkeye 1 observations presented by Kurth et al. [1975] also gave similar results.

Using RAE 2 in orbit about the moon, Kaiser and Alexander [1975] produced two-dimensional source location measurements of AKR from lunar occultations. They found that although the average source location at 250 kHz is between 2 to 3 R_e above the polar regions, a number of events indicate that the radiation may occasionally be generated at large radial distances (> 7 R_e). From single lunar occultations Alexander and Kaiser [1976] have observed several source regions at the same frequency. The most intense component of the multiple sources, they report, is almost always closest to the earth and the weakest component is the most distant. In addition, the sources in the northern hemisphere, on the night side, appear to trace out a 70° invariant latitude magnetic field line. A preliminary investigation by Alexander and Kaiser [1976] of the variation of source positions with observing frequency indicated that AKR emission at frequencies above 300 kHz came from closer to the earth than the emissions at frequencies less than 250 kHz.

The purpose of this paper is to determine the angular distribution of auroral kilometric radiation at different frequencies making use of observations from three satellites over a period of several years. Variations in these observed angular distributions as a

function of frequency are explored in order to try to obtain more information on the spatial position and characteristics of the source of the auroral kilometric radiation. The results of this survey are compared with ray tracing calculations for several proposed methods of generating this radiation.

II. METHOD OF ANALYSIS

A. Instrumentation

The University of Iowa has nearly identical plasma wave experiments onboard Hawkeye 1, IMP 6, and IMP 8. IMP 6 and Hawkeye 1 are in highly elliptical earth orbits. The apogee of Hawkeye 1 is over the north polar region at a radial distance of 130,856 km. The apogee of IMP 6 is nearer to the equatorial plane (orbit inclination of 28.7°) at a radial distance of 212,630 km. IMP 8 is in a slightly elliptic earth orbit near the equatorial plane with initial perigee and apogee radial distances of 147,434 and 295,054 km respectively and an orbit inclination of 28.6°.

Each of the three satellites has a long dipole antenna which is used for electric field measurements. The Hawkeye 1 antenna is the shortest measuring 41.8 meters from tip-to-tip. The IMP 6 and the IMP 8 antenna are longer, 92.5 meters and 121.8 meters tip-to-tip, respectively. To determine the electric field intensity at various frequencies the antenna signals are periodically analyzed with spectrum analyzers. The IMP 6 spectrum analyzer has 16 frequency bands with center frequencies from 36 Hz to 178 kHz. For this experiment the filter bandwidths range from about $\pm$ 10% of the center frequency at high frequencies to $\pm$ 20% at low frequencies. The electric field spectrum analyzers onboard Hawkeye 1 and IMP 8 also have 16 narrow band

frequency channels with center frequencies from 1.78 Hz to 178 kHz (± 10%) and 40 Hz to 178 kHz (± 10%) respectively. In addition, IMP 8 has a tunable wide band receiver which measures the electric field intensity at 2 MHz, 500, 125, or 31.1 kHz with a bandwidth of ± 1 kHz. The tunable wide band receiver on IMP 8 and each spectrum analyzer channel on Hawkeye 1, IMP 6, and IMP 8 has a dynamic range of about 100 db. The raw data from these spectrum analyzers are output voltages which range from 0 to 5 volts and are approximately proportional to the log of the actual voltage across the dipole antennas.

In 6 months Hawkeye 1 covers 24 hours of magnetic local time and provides observations from over the northern polar regions. Complete coverage of magnetic latitudes between -45° and +45° at all magnetic local times (out to 33 R_e) is accomplished by IMP 6 after one year in orbit. The magnetic latitudinal coverage of IMP 6 and IMP 8 are quite similar but a larger body of data is now available from IMP 6. Consequently observations from IMP 6 and Hawkeye 1 will be combined to determine the angular extent of auroral kilometric radiation at 56.2, 100, and 178 kHz in the northern hemisphere. Additional coverage by IMP 8 at 500 kHz will also be presented.

B. Cross Calibration of Hawkeye 1 and IMP 6

Since data from two different satellites, IMP 6 and Hawkeye 1, are to be combined in a single frequency of occurrence analysis it is desirable to perform a cross calibration of the two instrument sensitivities to make certain that no systematic differences are present in the calibrations. A convenient method of performing such a cross

calibration is to compare simultaneous observations of a type III solar radio burst. Type III bursts are radio emissions from the interaction of the interplanetary medium with superthermal electrons emitted from the sun during a flare [Lin, 1970]. The use of the type III bursts to provide a cross calibration of Hawkeye 1 and IMP 6 is based on the assumption that differences in the distances between the satellites and the origin of the type III burst is negligible compared to the distance the radiation has to travel to either of the satellites. Both satellites are then subjected to the same power flux.

Figure 1 shows a series of simultaneous observations of type III solar radio bursts by IMP 6 and Hawkeye 1 at 100 and 56.2 kHz on September 18, 1974, and at 178 kHz on September 17, 1974. The signature of a type III burst at these frequencies can be recognized easily as a smooth rapid increase in signal strength to a maximum on a time scale of a few minutes, then a gradual decrease to the receiver noise level on a time scale of several tens of minutes. Note the multiple type III event on September 17, 1974, in the 178 kHz channels. The large sporadic fluctuations on either side of the multiple type III are bursts of AKR. Close examination shows that the two satellites are tracking the same AKR bursts as is evident in the simultaneous rise and fall in the electric field strength in the 178 kHz channels.

The cross calibration graphs on the left of Figure 1 are obtained by plotting the raw voltage output of Hawkeye's spectrum

analyzer versus the raw voltage output of IMP 6's analyzer for these type III bursts. Each point is a measurement from both satellites taken at the same time and at the same frequency during the slowly decreasing part of the type III radio signal. Only the peaks in the measurements were used to take into account the obvious spin modulation. From the line in each graph the relationship between the output voltage from the receivers on Hawkeye 1 and IMP 6 can be found. These output voltages are assumed to correspond to the same power flux. The slope of each line is unity, confirming that the sensitivity of each receiver is identical. The in-flight calibration curves agree within 2 db of the preflight calibrations.

III. ANGULAR DISTRIBUTION OF AURORAL KILOMETRIC RADIATION

Inference of an angular distribution can be made by examining where the satellites have observed the highest frequency of occurrence of auroral kilometric radiation. A two dimensional frequency of occurrence diagram of AKR can be constructed in magnetic latitude (λ_m) and magnetic local time (MLT) by using a R^{-2} (R is the distance from the source to the observer) power flux threshold criteria to account for the expected $1/R^2$ radial variations of the power flux [see Gurnett, 1974]. Such a threshold enables a satellite, in principle, to observe the same intensity AKR bursts anywhere in its orbit.

Based on a survey of ten months of Hawkeye 1 data at 178, 100, and 56.2 kHz and one and a half years of IMP 8 data at 500 kHz a power flux threshold was chosen to be 25 db below the maximum power flux observed for each frequency. This threshold is determined by the conflicting requirements to obtain enough data points above the threshold for good statistical accuracy while still assuring that the threshold is well above the receiver noise for each spacecraft and at each of the frequencies analyzed. The thresholds selected are as follows:

$$(500\ \text{kHz})\ \text{Threshold} = (R_e/R)^2 \times (2.17 \times 10^{-16})\ \text{watts m}^{-2}\ \text{Hz}^{-1}$$

$$(178\ \text{kHz})\ \text{Threshold} = (R_e/R)^2 \times (7.35 \times 10^{-16})\ \text{watts m}^{-2}\ \text{Hz}^{-1}$$

$$(100\ \text{kHz})\ \text{Threshold} = (R_e/R)^2 \times (7.32 \times 10^{-16})\ \text{watts m}^{-2}\ \text{Hz}^{-1}$$

$$(56.2\ \text{kHz})\ \text{Threshold} = (R_e/R)^2 \times (2.59 \times 10^{-16})\ \text{watts m}^{-2}\ \text{Hz}^{-1}$$

Since the distance from the spacecraft to the source(s) of auroral kilometric radiation is not known during the initial reduction of data, the R value used in calculating the power flux threshold is the geocentric radial distance to the spacecraft. To reduce the error caused by the uncertainty in the radial distance to the source and to avoid complications due to near earth propagation effects only measurements obtained at $R > 7\ R_e$ are used in the analysis. If the source is near the earth ($R < 3\ R_e$), then the uncertainty in the radial distance correction to the threshold is at most $\pm$ 4 db, which is small compared to the amplitude range ($\sim$ 100 db) over which the intensity of AKR varies.

The frequency of occurrence diagram determined from the frequency of occurrence analysis for 56.2 kHz is shown in Figure 2. The measurements used comprise 3.5 years of IMP 6 data and 10 months of Hawkeye 1 data. Block of 5° increments in λ_m and 2 hour increments of MLT are used. The magnetic coordinates of the spacecraft determines which block an observation is made in. In each block the total number of three minute observations of AKR are divided by the total number of three minute observations in that block to give the frequency of occurrence. Local midnight is at the center of the abscissa and the

black shading represents the highest percentage of possible times that AKR was detected above the set power flux threshold. Evident in Figure 2 is the distinct filled emission cone (black shading) of AKR in the northern hemisphere. The emission cone appears to be symmetric about 22 hours magnetic local time indicating that the preferred direction of AKR is in the local evening which is in agreement with direction finding measurements of the average source(s) location(s) [Kurth et al., 1975; Kaiser and Stone, 1975]. A complicated frequency of occurrence pattern (line and dot shading) exists at low latitudes near local midnight. At high magnetic latitudes on the day side of the earth (6 to 10 hours MLT) the frequency of occurrence of AKR changes by at least a factor of 4 at $\lambda_m = 65° \pm 10°$. This rapid change in the frequency of occurrence indicates that a relatively stable boundary to the AKR angular distribution occurs on the day side of the earth.

The frequency of occurrence diagrams at 100 and 178 kHz, produced in the same manner as Figure 2, are shown in Figures 3 and 4 respectively. The same basic features of the AKR angular distribution as were pointed out in Figure 2 are evident with the exception of one significant difference. At higher frequencies (particularly 178 kHz) the cone of emission (black shading) has a large solid angle and extends closer to the magnetic equator at local midnight.

Figure 5 shows the frequency of occurrence of AKR at 500 kHz from one and a half years of IMP 8 data. Hawkeye 1 and IMP 6 do not have a 500 kHz channel, consequently we are limited in latitudinal

coverage to $\pm$ 45° λ_m. Figures 2, 3, 4, and 5 are consistent with the picture that from 56.2 to 500 kHz the solid angle of the emission cones increases as the frequency increases. At 500 kHz the northern and southern emission cones overlap substantially in the region near local midnight.

To obtain a clear idea as to where AKR is observed, on the average, we can normalize each of the frequency of occurrence diagrams. The normalization is accomplished by changing the scale of each frequency of occurrence diagram to a scale that ranges from zero to one where the maximum percent of occurrence equals one. Figure 6 shows the normalized percentage of observed auroral kilometric radiation for the three frequencies 178, 100, and 56.2 kHz versus magnetic latitude. All observations on the day side of the earth with magnetic local times between 8 hours and 12 hours are on the left hand side. The right hand side has night time observations from 20 to 24 hours magnetic local time. The observations are organized in magnetic latitude. The north magnetic pole is directly at the center of each plot. From 90° λ_m the normalized occurrence of AKR drops rapidly on the day side to less than 0.1 at 40° λ_m for each frequency. On the night side the normalized occurrence drops rapidly at 100 and 56.2 kHz and less rapidly at 178 kHz but to a higher value (about 0.4 at 0° λ_m) than the day side drop. This day-night skewness in the normalized occurrence of AKR, evident in Figure 6, could be produced by an angular distribution that would be variable in time on the night side and relatively well defined in time on the day side.

A picture of where auroral kilometric radiation is beamed can be constructed by noting the magnetic latitude of the normalized half occurrence points at all magnetic local times. The boundaries of the shaded areas in Figure 7 show the position of these normalized half occurrence points in magnetic coordinates. This illustration shows that AKR is preferentially beamed into larger solid angles at higher frequencies, approximately 1.1 steradians at 56.2 kHz, 1.8 steradians at 100 kHz, and 3.5 steradians at 178 kHz.

IV. SIMULTANEOUS OBSERVATIONS AT WIDELY SEPARATED LOCATIONS

Simultaneous observations from two satellites at widely separated locations reveal many important characteristics of auroral kilometric radiation that cannot be discerned with a single satellite. One of the most important questions which can be investigated is whether or not individual bursts of AKR simultaneously and uniformly illuminate the large solid angles depicted in Figure 7 or whether these frequency of occurrence distributions could be the result of a much narrower instantaneous beam or cone which varies in time.

To illustrate, Figure 8 presents simultaneous observations of IMP 6 and Hawkeye 1 electric field data for the same auroral kilometric storms. On the left hand side of this figure the corresponding frequencies from each satellite are individually compared in plots of electric field intensity versus time. It is easy to see that both satellites are observing radiation originating from the same source(s). On the right side, the satellite trajectories in MLT and λ_m coordinates are shown over the corresponding time period of the electric field observations. Figure 8 illustrates that individual AKR bursts are found to radiate in large solid angles and that the frequency of occurrence diagrams are not representations of small solid angle beams of auroral kilometric radiation that have moved in time. In addition the absolute power fluxes of AKR observed by both satellites are nearly

identical (to within about 2 db). This important observation indicates that the source(s) of auroral kilometric radiation uniformly illuminates the emission cones.

Simultaneous observations of electric field data from IMP 8 and Hawkeye 1 can be used to investigate propagation cutoffs characteristic of auroral kilometric radiation. In Figure 9, for instance, IMP 8 is near three hours magnetic local time at large radial distances and is observing intense storms of auroral kilometric radiation during the entire time period shown. Hawkeye 1 also observes these intense storms of AKR but only in certain regions of its orbit. This is evidently a spatial effect and not a temporal effect since IMP 8 still observes AKR when Hawkeye 1 is out of the emission cone.

The position of the plasmapause in Figure 9 has been identified by the change in the low frequency (17.8 Hz) electric field intensity and the plasmaspheric hiss cutoff, similar to the observations of Shaw and Gurnett [1975]. The identification of the upper hybrid resonance (UHR) noise in Figure 9 also provides an indication of the location of the plasmapause boundary.

In Figure 9 the position of the plasmapause at 1252 UT (Universal Time) closely corresponds to the abrupt drop in intensity of AKR as observed from Hawkeye 1 near local midnight. The times of the signal loss for the different frequencies (178, 100 and 56.2 kHz) are not the same. At higher frequencies the propagation cutoff tends to occur closer to the earth. This same characteristic of AKR at low altitudes on the night side has been previously reported by Gurnett

[1974] from IMP 6 data. Gurnett [1974] notes that the propagation cutoffs of AKR are consistent with the expected rapid increase in the plasma density at the plasmapause. The higher frequencies propagate to depths of larger number densities before the rapid decrease in the amplitude of the noise occurs. This implies that the extent of the propagation of AKR on the night side is limited by the local plasma characteristics near the plasmapause.

At 1403 UT in Figure 9, Hawkeye 1 again leaves the plasmapause. As the spacecraft travels upward in its trajectory on the day side of the earth the intensity of the AKR gradually begins to increase over a distance of several R_e. IMP 8 meanwhile observes many large amplitude bursts of AKR at its position on the night side. The absences of an abrupt propagation cutoff on the day side of the earth indicates that the latitudinal boundary of the illumination region is not determined by the plasma characteristics near the plasmapause, in direct contrast with what is observed on the night side. This asymmetry in the angular distribution in the noon-midnight meridian provides important information about the propagation of auroral kilometric radiation at low altitudes (3 to 5 R_e). Any meaningful model of AKR ray paths must describe this effect.

V. COMPARISON OF RAY TRACING FROM TWO AKR GENERATION MECHANISMS

Ray tracing has been used to confirm existing theories on the properties of VLF and ELF phenomena in the magnetosphere such as whistlers [Kimura, 1966; Edgar and Smith, 1966]. Ray tracing different theories on the generation of AKR and comparing the results with the observed angular distribution presented in this paper is an excellent method of testing the validity of the proposed emission mechanisms. It will be shown in this study that the ray paths are very sensitive to source locations.

A. Generation Mechanisms

Observations of auroral kilometric radiation such as source location, frequency range, power level, beaming, and polarization must be incorporated into any realistic theoretical model. Of these, the polarization of AKR has not been measured. Models have been proposed such that the polarization of the resultant radiation is in either of the modes R-X or L-O. Table 1 gives a brief summary of characteristics of the proposed generation mechanisms and those observed for AKR.

We can use the ray tracing technique to test the beaming and propagation characteristics of the resultant electromagnetic emission produced from these mechanisms. As an initial effort to examine the

plausibility of the proposed emission mechanisms for auroral kilometric radiation this paper will consider only the results of ray tracing from the $3f_g/2$ mechanism and the doppler shift emission. Both of these mechanisms produce electromagnetic radiation in the R-X mode.

B. The Plasma Density Models

The polar magnetosphere and plasmapause are highly variable during magnetic storms. Auroral kilometric radiation is observed most frequently during these times of disturbed geomagnetic activity [Dunckel et al., 1970 and Gurnett, 1974]. In addition, the position of the plasmapause plays an important role in the angular extent of AKR on the night side (Figure 9). Two model magnetospheres will be used to take into account the variability in the size of the plasmapause.

During moderate magnetic activity the plasmapause has been reported to be located between 3.0 and 4.5 R_e in the equatorial plane [Carpenter, 1963]. Model I (top panel) in Figure 10, shows the electron densities used in the ray tracing program to represent times of moderate activity. Near times of severe magnetic storms the plasmapause contracts and may lie between 2.5 and 3.5 R_e [Carpenter, 1963]. Model II (Figure 10) represents severe magnetic storm times. Each model uses an ideal dipole magnetic field, symmetric about the dipole axis. Only the electron distributions in the northern hemisphere on the night side are shown in Figure 10.

Experimental justification for some of the density contours in Models I and II can be found in Figure 9. The UHR noise band in Figure 9 has a frequency range that extends between the local plasma

frequency and the local upper hybrid resonance frequency [Shaw and Gurnett, 1975]. From the position of the plasmapause determined by the peak in the 17.8 Hz channel in Figure 9 and the frequency range of the UHR noise the plasma frequency associated with the plasmapause boundary is between 56.2 and 100 kHz. A definition of the plasmapause corresponding to the 100 cm^{-3} density contour (electron plasma frequency of about 90 kHz) in Models I and II is then consistent with observation. From Figure 9, the position of the plasmapause on the day side is approximately 3.3 R_e at 18.6° λ_m. The plasmapause (100 cm^{-3} density) in Model II at 18.6° λ_m is also 3.3 R_e. From Figure 9, on the night side, the plasmapause is at approximately 3.87 R_e at 17.8° λ_m which is half way between the Model I and II plasmapause positions.

C. Program Description

A ray tracing computer program developed by Shawhan [1966, 1967a, 1967b] can be adapted to determine propagation characteristics of auroral kilometric radiation. The program is based on a closed set of first order differential equations in spherical polar coordinates derived by Haselgrove [1955] and Haselgrove and Haselgrove [1960]. These equations were specialized by Shawhan [1966] for ray tracing in a magnetic meridian for a model magnetosphere. The expressions for the phase index of refraction and its derivatives are in the cold plasma formulation by Stix [1962]. The behavior of a ray's path is determined from the following initial conditions; the frequency of the wave, initial wave normal angle, initial latitude, initial altitude, propagation mode, and the magnetospheric model.

D. Ray Tracing Results

Tracing of rays from the $3f_g/2$ source region in the noon midnight meridian at the four frequencies 500, 178, 100, and 56.2 kHz was done in the plasma density Model I and Model II. The results are shown in Figures 11 and 12. This mechanism is gyrorelated and the source position doesn't depend on the magnetospheric electron density model used. All the source locations are in the midnight meridian and are determined by finding the position on a 70° invariant latitude magnetic field line where the frequency of the observed radiation is equal to $3f_g/2$. This places the sources with frequencies of 500, 178, 100, and 56.2 kHz at radial distances from the earth of 1.69, 2.36, 2.83, and 3.38 R_e respectively. The 70° invariant latitude field line is used to be consistent with the observations of actual AKR source locations made by Alexander and Kaiser [1976]. Each source region is assumed to emit electromagnetic radiation in all directions. The sense of the initial wave normal angle (ψ) is such that when the direction of the phase velocity of the wave is parallel to the magnetic field direction $\psi = 180°$. Increments of 5° were used in the wave normal angles. Figures 11 and 12 show only the rays which give the furthest extent of the radiation and other representative rays which are of interest.

Ray paths generated in the Model I magnetosphere (plasmapause L value of 4.6) are shown in Figure 11. The day side extent of the rays are qualitatively what is observed; the higher the frequency, the lower the magnetic latitude at which the radiation can be observed. Note the rays on the night side penetrate the plasmapause to depths quali-

tatively consistent with Figure 9. These ray paths show that the plasmapause presents a refracting layer. Ray behavior in the Model II magnetosphere (plasmapause L value of 3.6) is illustrated in Figure 12. The angular extent of the day side rays are the same as for Figure 11. The substantial change in the angular distribution on the night side demonstrates that the position of the plasmapause, for this source location, reshapes the latitudinal penetration of the ray paths. The smaller plasmapause has allowed the rays to propagate down to the equatorial plane on the night side.

A comparison of this theoretical generation mechanism and the observational results of the angular extent of AKR is made in Table 2. This table shows that at 7 R_e, on the day side, the edges of the average cones of AKR (from Figure 7) are nearly equal to the maximum excursion of the ray paths of the $3f_g/2$ emission (from Figure 11 or 12). There is no large variation in the observed angular extent of AKR on the day side over 8 hours of MLT centered on the noon meridian. The night side extent of AKR from Table 2 has a variation of 15° or more at a specific frequency over a few hours of MLT. The actual size of the plasmapause in the equatorial plane is not only variable during magnetic activity but also is dependent on local time [Carpenter, 1970]. The evening bulge, as reported by Carpenter [1970], is situated from 20 hours MLT to 18 hours MLT. The extent of AKR at 20 to 22 hours MLT is similar to the extent of the rays paths of the $3f_g/2$ emission in the plasma density Model I; coincident with a bulge in the plasmapause. Ray paths from the $3f_g/2$ emission in Model II (Figure 12) are qualitatively

similar to the AKR extent from 0 to 2 hours MLT; coincident with a depression of the plasmapause.

The second generation mechanism to be considered here is produced by the doppler shift of 10 keV electrons at the electron gyrofrequency. The 10 keV electrons produce a 2% doppler shift in their emitted cyclotron frequency due to their velocity with respect to the rest frame of the magnetosphere. The source locations are determined by assuming that the frequency of the wave is at 1.02 times the local electron gyrofrequency (f_g) along a 70° invariant latitude field line. An electromagnetic wave with a frequency of 178 kHz would be generated at 2.10 R_e by this mechanism.

The top panel in Figure 13 shows the ray paths which make up the angular distribution of doppler shifted gyro emission of 10 keV electrons at 178 kHz. The ray path distribution is the same for both Model I and II plasma densities because all the rays are reflected very close to the assumed source region at or near the R = 0 cutoff. Since this source region is at low altitudes (very close to the R = 0 cutoff), the differing plasmapause location has no influence on the localized source region. Note that the angular distribution from this mechanism is not in good agreement with the observed angular distribution of AKR at 178 kHz (compare with Figure 12 at 178 kHz). Rays do not penetrate into the day side nor into the night side equatorial regions at large radial distances.

VI. DISCUSSION

The $3f_g/2$ mechanism produces ray paths in a model magnetosphere that qualitatively match the angular distribution of auroral kilometric radiation. It produces rays on the day side whose angular extent are determined from the plasma characteristics near the source. The extent of the rays on the night side is determined by the position of the plasmapause. The $3f_g/2$ mechanism, however, has one serious drawback. From power considerations Gurnett [1974] reasons that the mechanism that produces AKR must be highly efficient ($\sim 1\%$) in the conversion of the energy of precipitating electrons into electromagnetic radiation. The actual coupling between $3f_g/2$ electrostatic waves and $3f_g/2$ electromagnetic waves has not been verified experimentally and it is believed to have low efficiency [K. Papadopoulos, personal communication with Shawhan, 1975].

The most important plasma model dependent aspect of ray tracing is the allowed frequency range of the emission produced by a generation mechanism. The generation mechanism specifies the polarization of the radiation and with the addition of a plasma density model the frequency range of the escaping radiation is determined. The generation mechanisms that were used for ray tracing in this paper produced radiation only in the R-X mode. The radial variation of the frequency of the R-X cutoff along a 70° invariant latitude field line in either

Model I or Model II magnetospheres is illustrated in Figure 13 (bottom panel) and Figure 14. The R = 0 cutoff is the same for both plasma models since the change in the size of the plasmasphere did not affect the electron densities at high latitudes. The dotted line in each figure gives the frequency range of the radiation emitted by each mechanism which is allowed to escape. The bottom panel of Figure 13 shows that 10 keV doppler shift emission is allowed from 160 to 410 kHz in Models I or II magnetospheres. The frequency range of the $3f_g/2$ emission (30 to 800 kHz) shown in Figure 14 is very similar to that observed for AKR as demonstrated in Table 1.

A model magnetosphere could be devised which would produce a frequency range for the doppler shift mechanism in agreement with the observed frequency range. The electron densities in the auroral regions for such a magnetosphere would have to be reduced such that the frequency of the R-X cutoff surface is below 1.02 times the local electron gyrofrequency from 20 kHz to 2 MHz. Very few measurements of high latitude, high altitude electron densities exist. If the magnetic field lines in the auroral regions are 'open' then reduced electron number densities in these regions may be possible. Even if the R-X cutoff becomes nearly equal to the electron gyrofrequency at 178 kHz the angular extent of the doppler shift emission on the day side would increase by less than 25°. An increase of over 50° in the day side extent of the doppler shift emission (see top panel of Figure 13) would be necessary for this emission to be consistent with the observed day side extent of AKR.

Regardless of the generation mechanism, if AKR is emitted in the R-X mode certain limits on the location of the source region can be made which produce the observed angular distribution within $\pm$ 5° from 178 kHz to 56.2 kHz. For instance, the cross hatched region in Figure 15 shows the relationship between source locations and emission frequencies that would produce day side rays whose extent are consistent with that observed for auroral kilometric radiation. These source locations are strongly dependent on their position relative to the R-X cutoff surface. Rays whose extent would maintain the observed boundaries of AKR on the night side would originate from the source region indicated by the dot pattern in Figure 15 (using Plasma Model II). The location of this source region is strongly dependent on the size of the night side plasmapause.

From the ray tracing we can see that more complete observations of auroral kilometric radiation are needed at higher frequencies (500 kHz). These higher frequencies will according to the $3f_g/2$ mechanism penetrate deeper into the plasmapause on the night side but will also have source regions much closer to the earth. The result is that the night side extent of these rays is not as great as that of the intermediate frequencies (100 or 178 kHz). The day side extent may eventually be determined by the day side plasmapause.

The proposed mechanisms for the generation of auroral kilometric radiation that are listed in Table 1 are unable to adequately explain the multiple source locations (some of which extend beyond 4 R_e) observed by Alexander and Kaiser [1976] at 250 kHz. It may be difficult

to determine if there are multiple sources at high frequencies (~ 500 kHz) from their angular distributions since from ray path considerations low altitude high frequency source locations should already produce large emission cones. Low frequency (< 200 kHz) sources, however, at large radial distances along an auroral field line would drastically increase the angular extent of their emission. The time averaged angular distributions of AKR at 178, 100, and 56.2 kHz presented in this paper can be qualitatively described by sources at low altitudes. This indicates that the multiple sources at radial distances greater than 4 R_e for these frequencies (178, 100, and 56.2 kHz) may exist only for such short periods of time that they do not contribute significantly to the frequency of occurrence, or the intensity of these sources are lower than the power flux thresholds used in this study.

VII. CONCLUSIONS

Analysis of spacecraft data from Hawkeye 1, IMP 6 and IMP 8 have hed to the following conclusions concerning the propagation characteristics of auroral kilometric radiation:

1) AKR in the northern hemisphere is beamed into a cone-shaped region whose solid angle increases with increasing frequency, varying from approximately 1.1 steradians at 56.2 kHz to approximately 3.5 steradians at 178 kHz.

2) There is simultaneous illumination with nearly constant intensities over the entire solid angle.

3) The symmetry axis of the emission cone is tilted toward local evening by about 20°.

4) There is a day-night asymmetry in the topside plasmapause cutoffs, with sharp cutoffs on the night side of the earth and no corresponding cutoff on the day side.

Ray tracing calculations for two proposed mechanisms using two magnetospheric density models lead to the following conclusions:

5) The $3f_g/2$ mechanism has an angular extent more consistent with the observed angular distribution than the 10 keV doppler shift mechanism.

6) Rays in the $3f_g/2$ mechanism exhibit the day-night asymmetry in the topside plasmapause cutoffs.

From general ray tracing considerations the angular distribution of AKR can be reproduced from low altitude source regions (from 2 to 3.5 R_e) along a 70° invariant latitude magnetic field line in the midnight meridian using emission in the R-X mode.

ACKNOWLEDGMENTS

The research at the University of Iowa was supported by the National Aeronautics and Space Administration through grants NGL-16-001-002 and NGL-16-001-043; through contracts NAS1-11257 and NAS1-13129 with Langley Research Center, and through contracts NAS5-11074, and NAS5-11431 with Goddard Space Center; by the Office of Naval Research, and by the National Science Foundation, Atmospheric Sciences Section.

TABLE 1

Basic Characteristics of AKR Compared to Those of Proposed Generation Mechanisms

	Frequency Range	Polarization	Coupling	Probable Peak Power Output	Special Conditions
AKR	20 kHz to 2 MHz	Unknown	Unknown	10^9 watts	Unknown
$3f_g/2$ (Gurnett, 1974; Scarf, 1974)	30 kHz to 800 kHz (from Model I or II)	R - X	ES → EM (R-X)	$< 10^9$ watts	$f_p < f_w$ ($= 3f_g/2$)
Doppler Shift of 10 keV electrons (Melrose, 1975)	160 kHz to 410 kHz (from Model I or II)	R - X	EM (R-X)	$< 10^9$ watts	$f_p < f_w$ ($= 1.02\ f_g$)
Direct Coupling Mechanism (Palmadesso et al., 1976)	20 kHz to 600 kHz (from Model I or II)	L - O	EIC → EM (L-O)	$\simeq 10^9$ watts	$f_g < f_w < f_{UHR}$
Indirect Coupling Mechanism (Benson, 1975)	12 kHz to 1 MHz (from Model I or II where $2f_g = f_{UHR}$)	L - O	ES → EM (X) → EM (L-O)	$\ll 10^9$ watts	$f_p \simeq f_w$

ES = Electrostatic Wave
EM = Electromagnetic Wave
EIC = Electrostatic Ion Cyclotron Wave
f_w = Frequency of the Resultant EM Wave
f_p = Plasma Frequency
f_g = Gyrofrequency
f_{UHR} = Upper Hybrid Resonance Frequency

TABLE 2

Comparison of the Ray Extent of $3f_g/2$ Mechanism with the Extent of AKR

Dayside Extent at 7 R_e

Frequency (in kHz)	Ray Tracing Results	Observations			
	Model I or Model II (Magnetic Latitude λm)	Magnetic Local Time (hours)			
		16 to 14	14 to 12	12 to 10	10 to 8
178	45°	50°	50°	55°	55°
100	60°	50°	65°	75°	75°
56.2	86°	70°	75°	75°	70°

Nightside Extent at 7 R_e

Frequency (in kHz)	Ray Tracing Results		Observations			
	Model I (in λ_m)	Model II (in λ_m)	Magnetic Local Time (hours)			
			20 to 22	22 to 24	0 to 2	2 to 4
178	20°	6°	20°	10°	5°	25°
100	18°	5°	45°	20°	35°	50°
56.2	21°	11°	50°	45°	50°	55°

REFERENCES

Ackerson, K. L. and L. A. Frank, Correlated satellite measurements of low-energy electron precipitation and ground-based observations of a visible auroral arc, J. Geophys. Res., 77, 1128, 1972.

Alexander, J. K. and M. L. Kaiser, Terrestrial kilometric radiation: 1-spatial structure studies, preprint, Goddard Space Flight Center X-693-76-47, 1976.

Benson, R. F., Source mechanism for terrestrial kilometric radiation, Geophys. Res. Lett., 2, 52, 1975.

Carpenter, D. L., Whistler evidence of a 'knee' in the magnetospheric ionization density profile, J. Geophys. Res., 68, 1675, 1963.

Carpenter, D. L., Whistler evidence of the dynamic behavior of the dusk side bulge in the plasmasphere, J. Geophys. Res., 75, 3837, 1970.

Dunckel, N., B. Ficklin, L. Rorden, and R. A. Helliwell, Low-frequency noise observed in the distant magnetosphere with OGO 1, J. Geophys. Res., 75, 1854, 1970.

Edgar, B. C. and R. L. Smith, Magnetospherically reflected whistlers in OGO-I, papers 4-12, 1966 URSI Meeting, December 14, 17, Stanford University.

Gurnett, D. A., The earth as a radio source: terrestrial kilometric radiation, J. Geophys. Res., 79, 4227, 1974.

Gurnett, D. A., The earth as a radio source: the non-thermal continuum, J. Geophys. Res., 80, 2751, 1975.

Haselgrove, J., Ray theory and a new method for ray tracing, London Physical Society, Report of Conference on the Physics of the Ionosphere, 355, 1955.

Haselgrove, C. G. and J. Haselgrove, Twisted ray paths in the ionosphere, Proc. Roy. Soc. London, 75, 357, 1960.

Kaiser, M. L. and J. E. Alexander, Source measurements of terrestrial kilometric radiation obtained from lunar orbit, Geophys. Res. Lett., 3, 37, 1976.

Kaiser, M. L. and R. G. Stone, Earth as an intense planetary radio source: similarities to Jupiter and Saturn, Science, 189, 285, 1975.

Kimura, I., Effects of ions on whistler-mode ray tracing, Radio Science, 1, (3) (new series), 269, 1966.

Kurth, W. S., M. M. Baumback, and D. A. Gurnett, Direction finding measurements of auroral kilometric radiation, J. Geophys. Res., 80, 2764, 1975.

Lin, R. P., The emission and propagation of ~ 40 keV solar flare electrons, Solar Phys., 12, 266-303, 1970.

Melrose, D. B., An interpretation of Jupiter's decametric radiation and the terrestrial kilometric radiation as direct amplified gyroemission, preprint, Astro-geophysics Department, University of Colorado, 1975.

Palmadesso, P., T. P. Coffey, S. L. Ossakow, and K. Papadopoulos, Generation of terrestrial kilometric radiation by a beam-driven electromagnetic instability, J. Geophys. Res., 81, 1762, 1976.

Scarf, Frederick L., A new model for the high frequency decametric radiation from Jupiter, J. Geophys. Res., 79, 3835, 1974.

Shaw, R. R. and D. A. Gurnett, Electrostatic noise bands associated with the electron gyrofrequency and plasma frequency in the outer magnetosphere, J. Geophys. Res., 80, 4259, 1975.

Shawhan, S. D., VLF ray tracing in a model ionosphere, Dept. Physics and Astronomy, U. of Iowa Res. Rept. 66-33, 1966.

Shawhan, S. D., A computer program for VLF ray tracing in a model ionosphere, Dept. Physics and Astronomy, U. of Iowa Res. Rept. 67-12, 1967a.

Shawhan, S. D., Behavior of VLF ray paths in the ionosphere, Dept. Physics and Astronomy, U. of Iowa Res. Rept. 67-25, 1967b.

Stix, T. H., The Theory of Plasma Waves, McGraw-Hill, New York, 1962.

FIGURE CAPTIONS

Figure 1 Cross-calibration of the receiver responses of the plasma wave experiments on Hawkeye 1 and IMP 6 by using simultaneous observations of a type III radio burst.

Figure 2 The frequency of occurrence diagram of auroral kilometric radiation as observed from IMP 6 and Hawkeye 1 spacecraft at 56.2 kHz as a function of magnetic local time and magnetic latitude.

Figure 3 The frequency of occurrence diagram of auroral kilometric radiation as observed from IMP 6 and Hawkeye 1 spacecraft at 100 kHz as a function of magnetic local time and magnetic latitude.

Figure 4 The frequency of occurrence diagram of auroral kilometric radiation as observed from IMP 6 and Hawkeye 1 spacecraft at 178 kHz as a function of magnetic local time and magnetic latitude.

Figure 5 The frequency of occurrence diagram of auroral kilometric radiation as observed from IMP 8 spacecraft at 500 kHz as a function of magnetic local time and magnetic latitude.

Figure 6 The normalized percent of occurrence of auroral kilometric radiation in magnetic meridian sections between 8 and 12 hours and 20 and 24 hours magnetic local time.

Figure 7 The latitudinal boundary of the auroral kilometric radiation emission cone at 178, 100, and 56.2 kHz in magnetic coordinates. The decreasing angular size of the emission region with decreasing frequency is clearly evident.

Figure 8 Simultaneous observations from Hawkeye 1 and IMP 6 spacecrafts of auroral kilometric radiation at widely separated magnetic latitudes. In this case the intensity variations are closely correlated, indicating that the radiation occurs simultaneously over a large solid angle. In addition the absolute power fluxes are approximately the same at both spacecraft.

Figure 9 IMP 8 is at large radial distances on the night side in the northern hemisphere observing intense bursts of AKR. Meanwhile, Hawkeye 1 moves in and out of the emission cones of AKR as it travels in its trajectory near the noon-midnight meridian. As observed from Hawkeye 1, the topside plasmapause acts as an abrupt propagation cutoff to AKR only on the night side. On the day side AKR doesn't propagate down to the topside plasmapause. The 17.8 Hz channel is used to determine the position of the plasmapause.

Figure 10 Two model magnetospheres used in the ray tracing of auroral kilometric radiation.

Figure 11 Ray tracing results of the $3f_g/2$ mechanism in the Model I magnetosphere at 500, 178, 100 and 56.2 kHz.

Figure 12 Ray tracing results of the $3f_g/2$ mechanism in the Model II magnetosphere at 500, 178, 100 and 56.2 kHz.

Figure 13 Top Panel: Ray tracing results of 10 keV doppler shift gyro emission in Model I or II magnetospheres at 178 kHz. Bottom Panel: The radial variation of the R-X cutoff frequency along a 70° invariant latitude magnetic field line in the Model I or II magnetospheres. The arrows indicate the frequency range of 10 keV doppler shift gyro emission.

Figure 14 The radial variation of the R-X cutoff frequency along the 70° invariant latitude magnetic field line in the Model I or II magnetospheres. The dotted line shows the frequency range of $3f_g/2$ electromagnetic radiation.

Figure 15 Source regions in the midnight meridian (along a 70° invariant latitude field line) which produce rays of frequencies 178 to 56.2 kHz in the R-X mode whose angular

extent is consistent with that observed for AKR as determined from the frequency of occurrence survey. The cross hatched indicates the source region determined from only the day side extent of AKR. The dot pattern indicates the source region determined from only the night side extent of AKR.

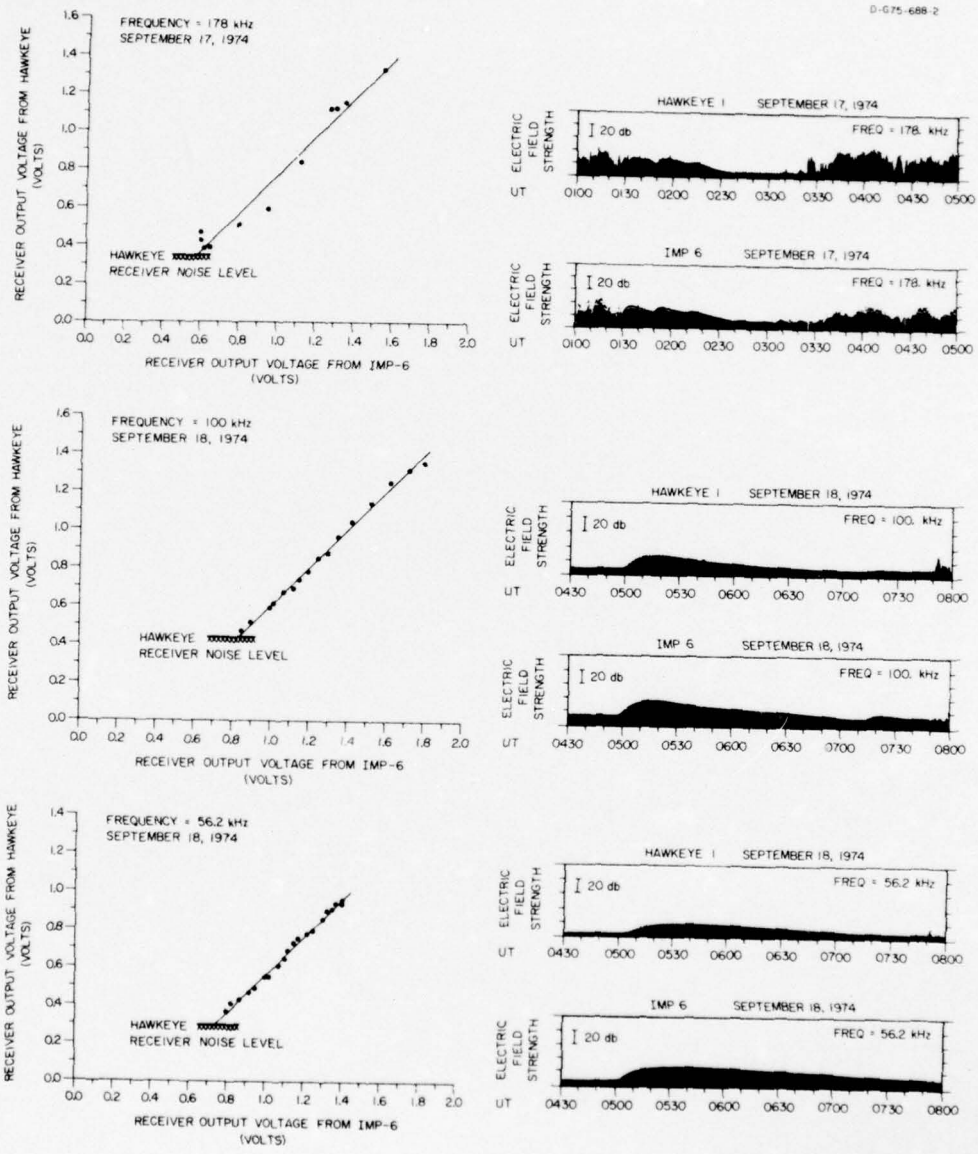
D-675-688-2
FREQUENCY = 178 kHz
SEPTEMBER 17, 1974
RECEIVER OUTPUT VOLTAGE FROM HAWKEYE (VOLTS)
HAWKEYE
RECEIVER NOISE LEVEL
RECEIVER OUTPUT VOLTAGE FROM IMP-6 (VOLTS)
HAWKEYE 1 SEPTEMBER 17, 1974
ELECTRIC FIELD STRENGTH
20 db
FREQ = 178. kHz
UT
0100 0130 0200 0230 0300 0330 0400 0430 0500
IMP 6 SEPTEMBER 17, 1974
FREQUENCY = 100 kHz
SEPTEMBER 18, 1974
HAWKEYE 1 SEPTEMBER 18, 1974
FREQ = 100. kHz
0430 0500 0530 0600 0630 0700 0730 0800
IMP 6 SEPTEMBER 18, 1974
FREQUENCY = 56.2 kHz
SEPTEMBER 18, 1974
HAWKEYE 1 SEPTEMBER 18, 1974
FREQ = 56.2 kHz
IMP 6 SEPTEMBER 18, 1974

Figure 1

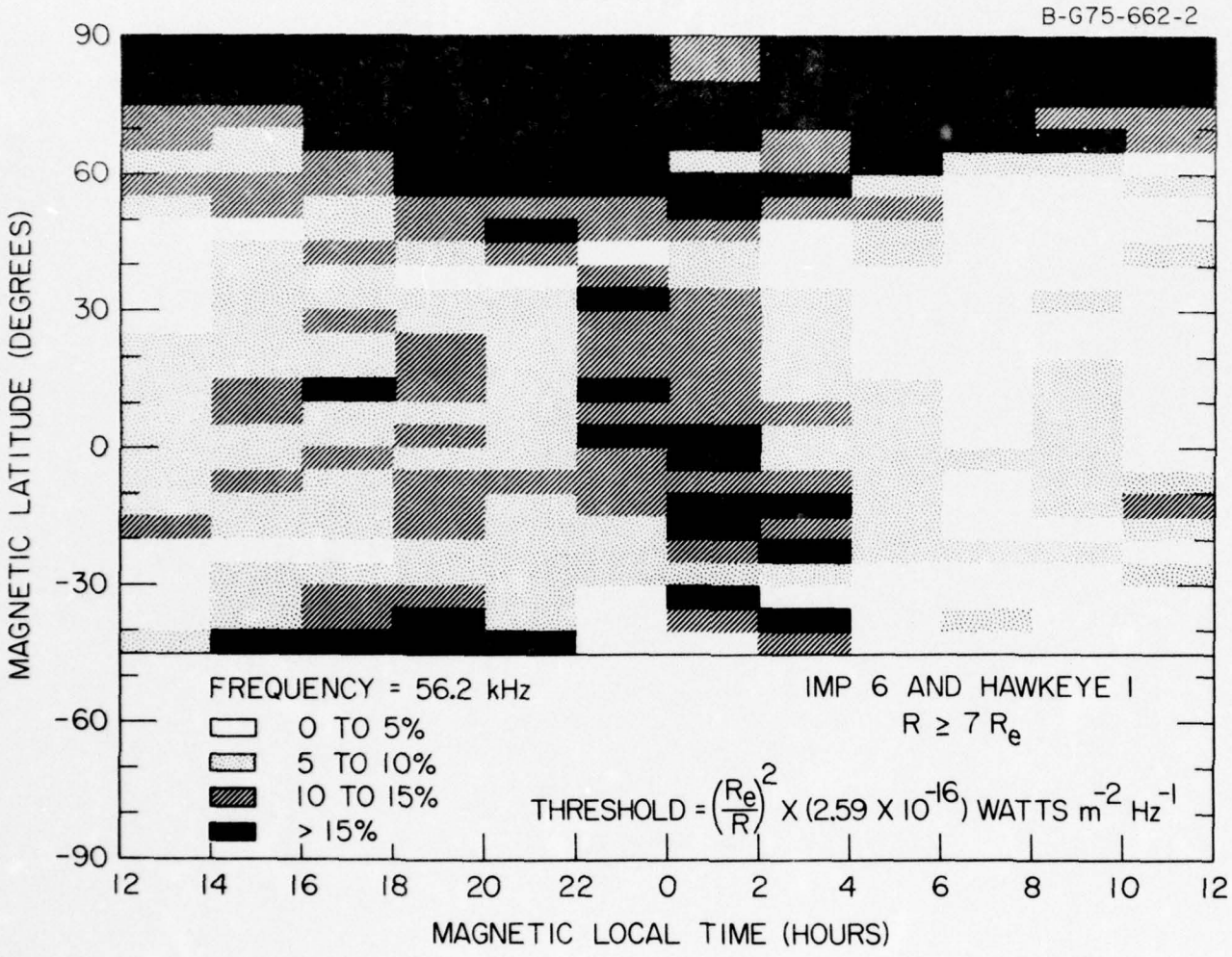
B-G75-662-2
90
60
30
0
-30
-60
-90
MAGNETIC LATITUDE (DEGREES)
FREQUENCY = 56.2 kHz
0 TO 5%
5 TO 10%
10 TO 15%
> 15%
IMP 6 AND HAWKEYE I
R ≥ 7 Re
THRESHOLD = (Re/R)^2 X (2.59 X 10^-16) WATTS m^-2 Hz^-1
12 14 16 18 20 22 0 2 4 6 8 10 12
MAGNETIC LOCAL TIME (HOURS)

Figure 2

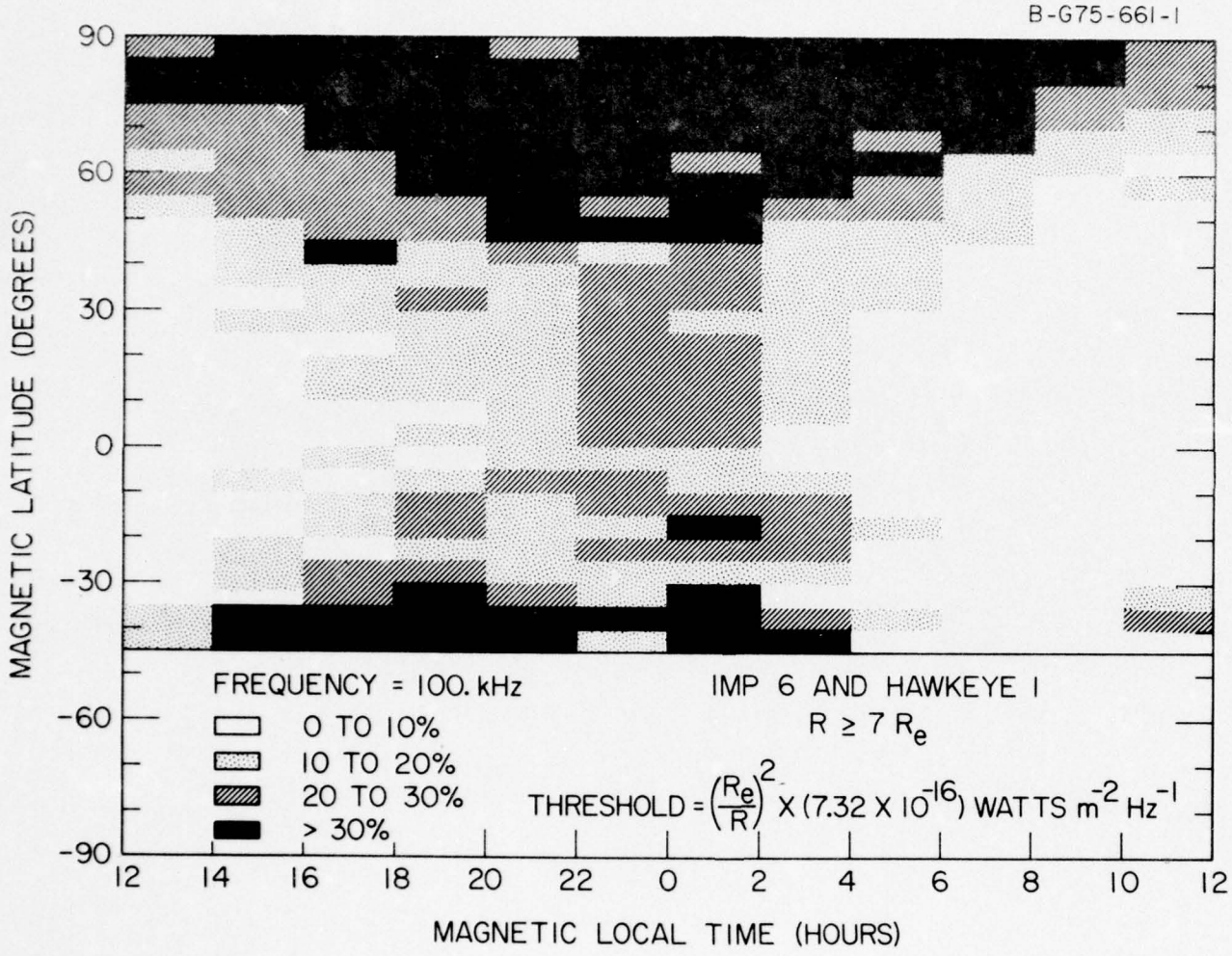
B-G75-661-1
90
60
30
0
-30
-60
-90
MAGNETIC LATITUDE (DEGREES)
FREQUENCY = 100. kHz
0 TO 10%
10 TO 20%
20 TO 30%
> 30%
IMP 6 AND HAWKEYE 1
R ≥ 7 Re
THRESHOLD = (Re/R)^2 X (7.32 X 10^-16) WATTS m^-2 Hz^-1
12
14
16
18
20
22
0
2
4
6
8
10
12
MAGNETIC LOCAL TIME (HOURS)

Figure 3

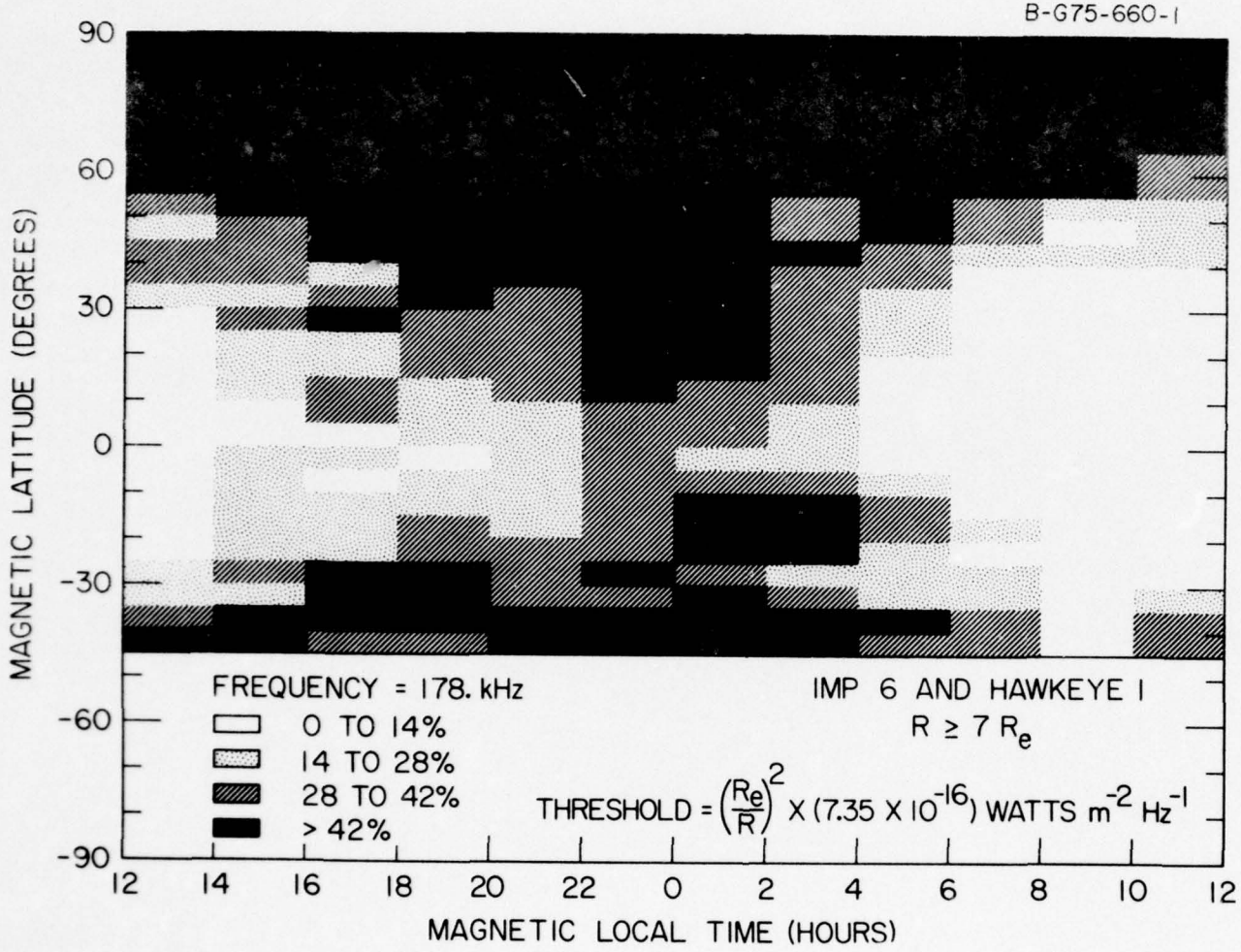
B-G75-660-1
90
60
30
0
-30
-60
-90
MAGNETIC LATITUDE (DEGREES)
FREQUENCY = 178. kHz
0 TO 14%
14 TO 28%
28 TO 42%
> 42%
IMP 6 AND HAWKEYE 1
R ≥ 7 Re
THRESHOLD = (Re/R)^2 X (7.35 X 10^-16) WATTS m^-2 Hz^-1
12 14 16 18 20 22 0 2 4 6 8 10 12
MAGNETIC LOCAL TIME (HOURS)

Figure 4

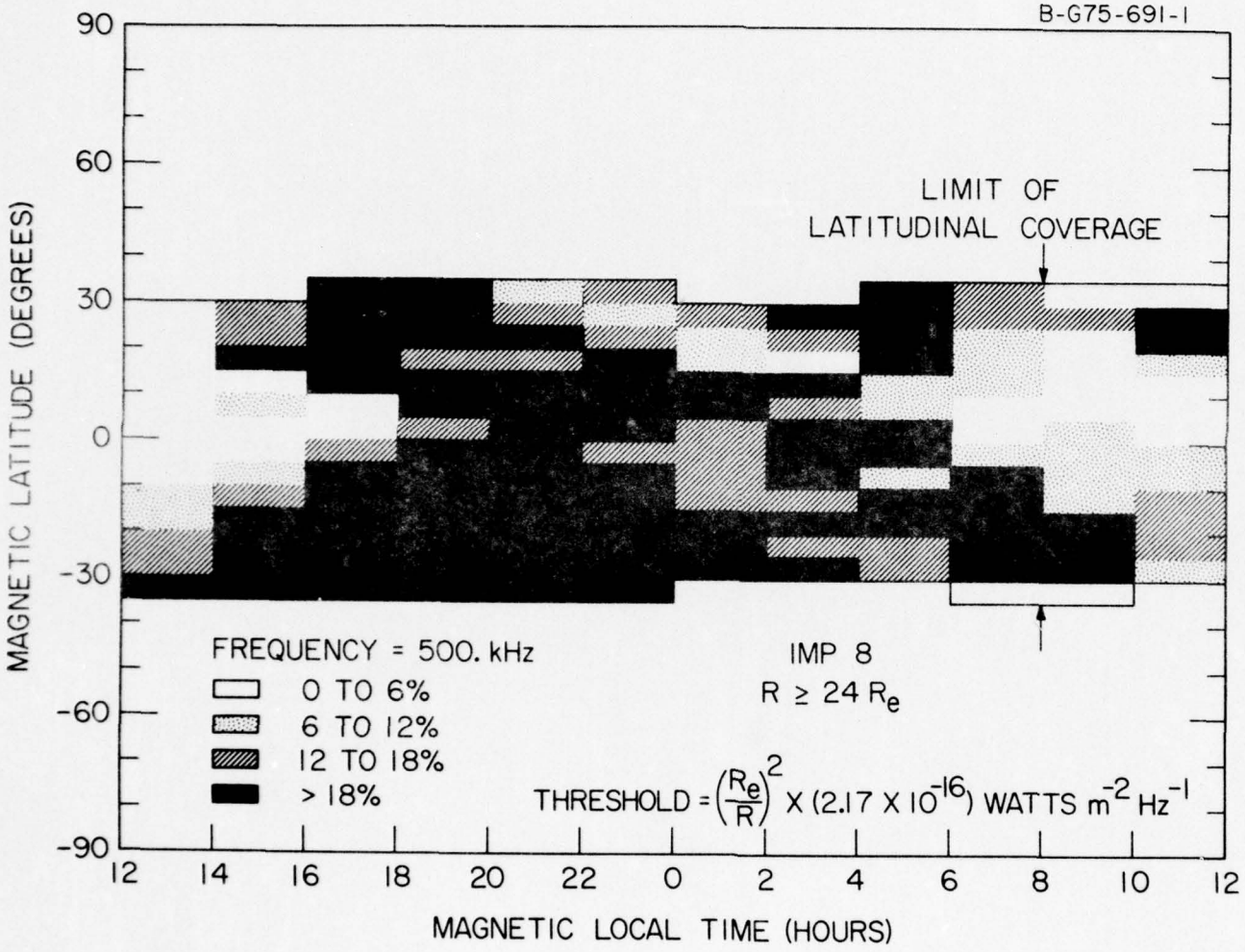
B-G75-691-1
90
60
30
0
-30
-60
-90
MAGNETIC LATITUDE (DEGREES)
LIMIT OF
LATITUDINAL COVERAGE
FREQUENCY = 500. kHz
0 TO 6%
6 TO 12%
12 TO 18%
> 18%
IMP 8
R ≥ 24 Re
THRESHOLD = (Re/R)^2 X (2.17 X 10^-16) WATTS m^-2 Hz^-1
12
14
16
18
20
22
0
2
4
6
8
10
12
MAGNETIC LOCAL TIME (HOURS)

Figure 5

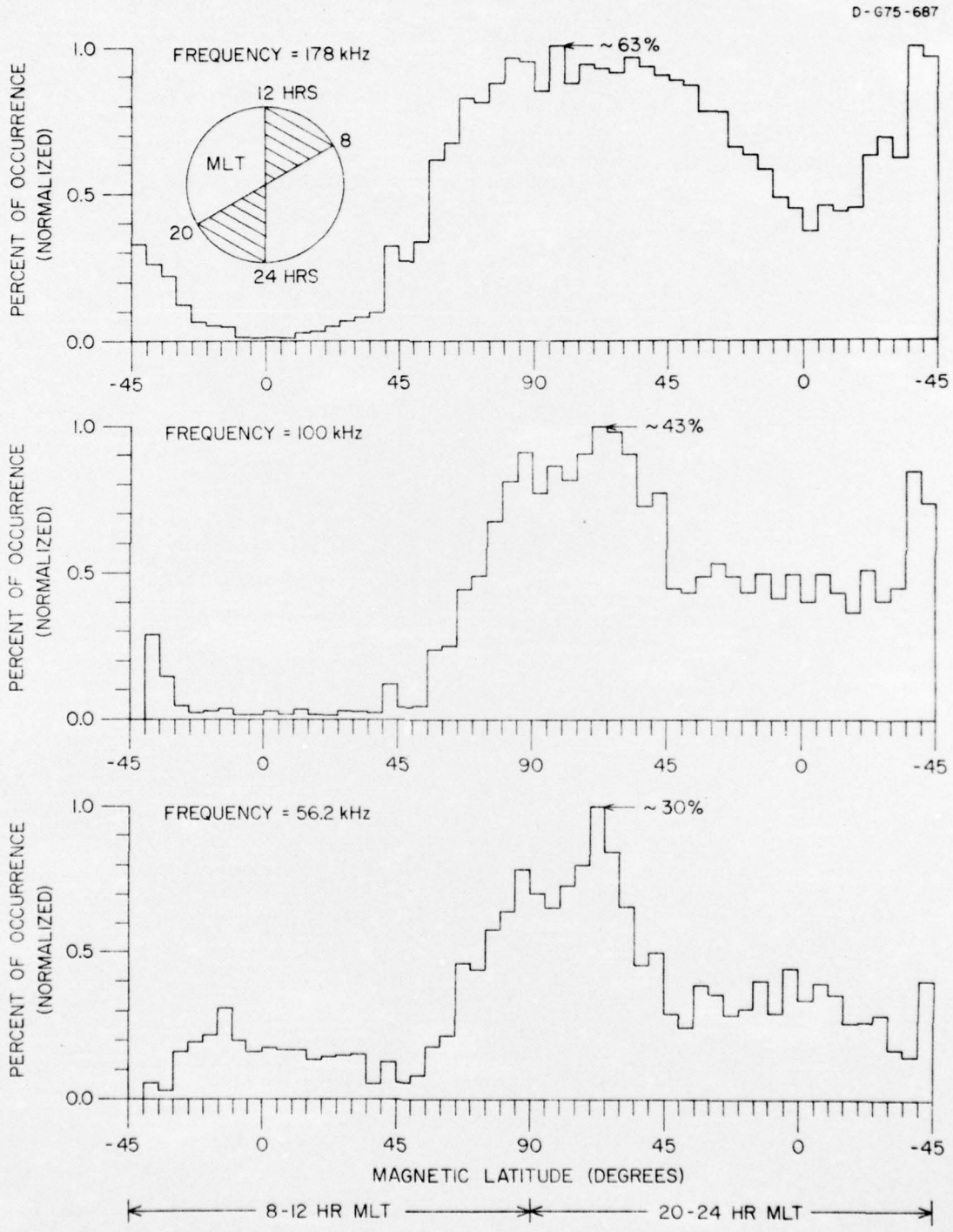
D-G75-687
FREQUENCY = 178 kHz
~63%
12 HRS
8
MLT
20
24 HRS
PERCENT OF OCCURRENCE (NORMALIZED)
1.0
0.5
0.0
-45
0
45
90
45
0
-45
FREQUENCY = 100 kHz
~43%
FREQUENCY = 56.2 kHz
~30%
MAGNETIC LATITUDE (DEGREES)
8-12 HR MLT
20-24 HR MLT

Figure 6

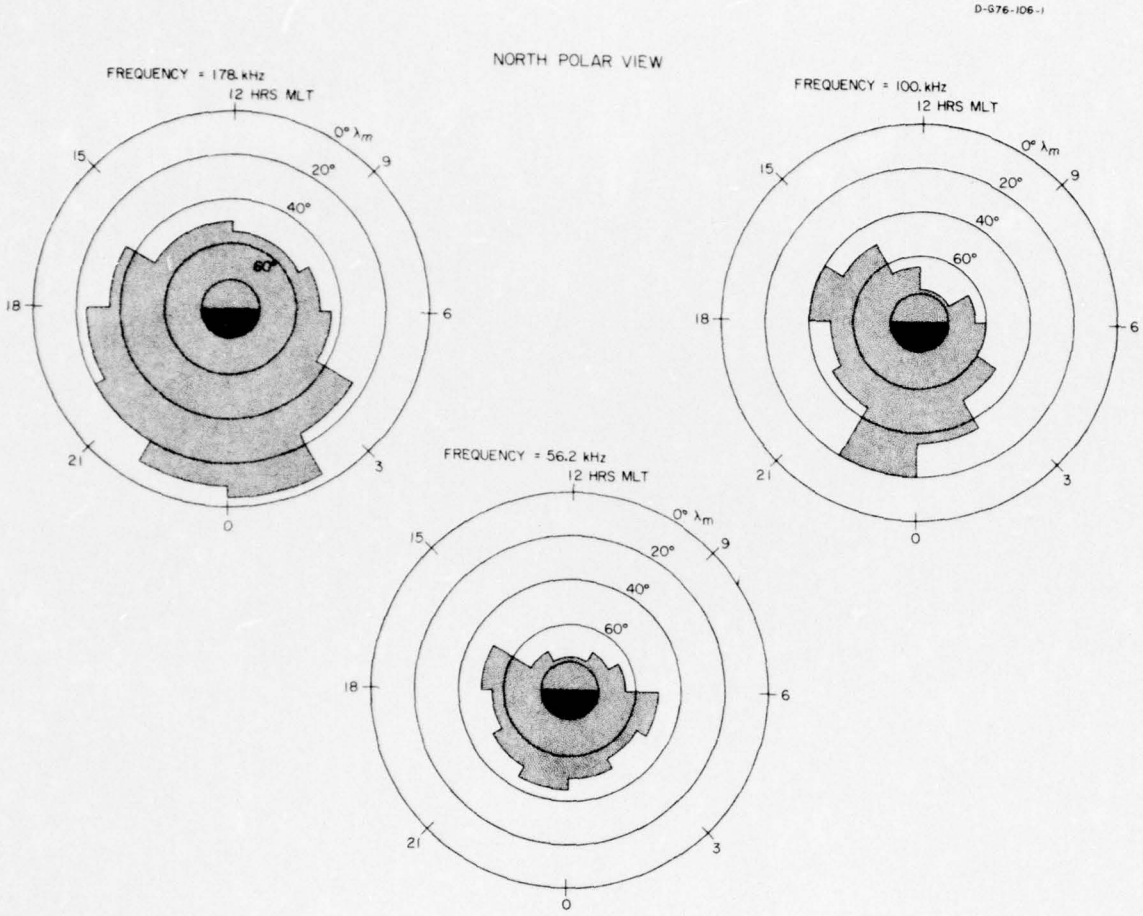
D-G76-106-1
NORTH POLAR VIEW
FREQUENCY = 178 kHz
12 HRS MLT
0° λm
20°
40°
60°
FREQUENCY = 100 kHz
12 HRS MLT
FREQUENCY = 56.2 kHz
12 HRS MLT
0
3
6
9
15
18
21

Figure 7

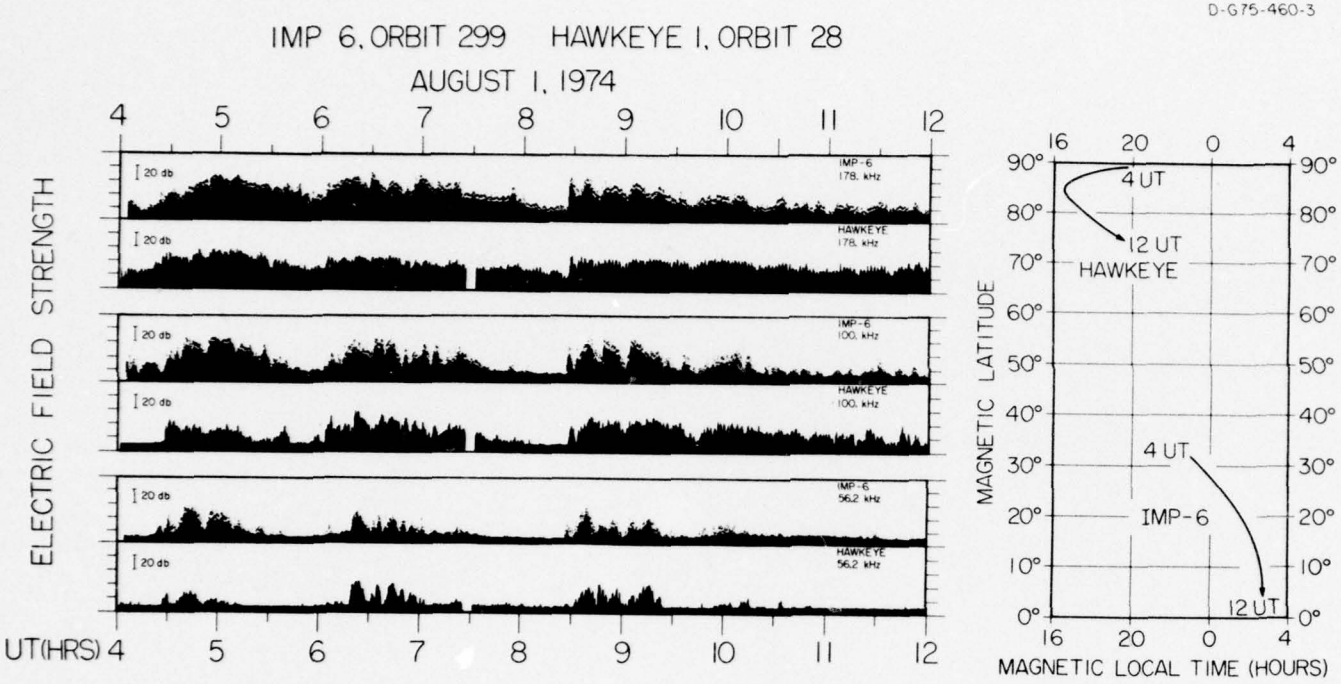
IMP 6, ORBIT 299 HAWKEYE 1, ORBIT 28
AUGUST 1, 1974
ELECTRIC FIELD STRENGTH
UT(HRS)
4
5
6
7
8
9
10
11
12
20 db
IMP-6
178. kHz
HAWKEYE
178. kHz
IMP-6
100. kHz
HAWKEYE
100. kHz
IMP-6
56.2 kHz
HAWKEYE
56.2 kHz
MAGNETIC LATITUDE
MAGNETIC LOCAL TIME (HOURS)
16
20
0
4
90°
80°
70°
60°
50°
40°
30°
20°
10°
0°
4 UT
12 UT
HAWKEYE
4 UT
IMP-6
12 UT

Figure 8

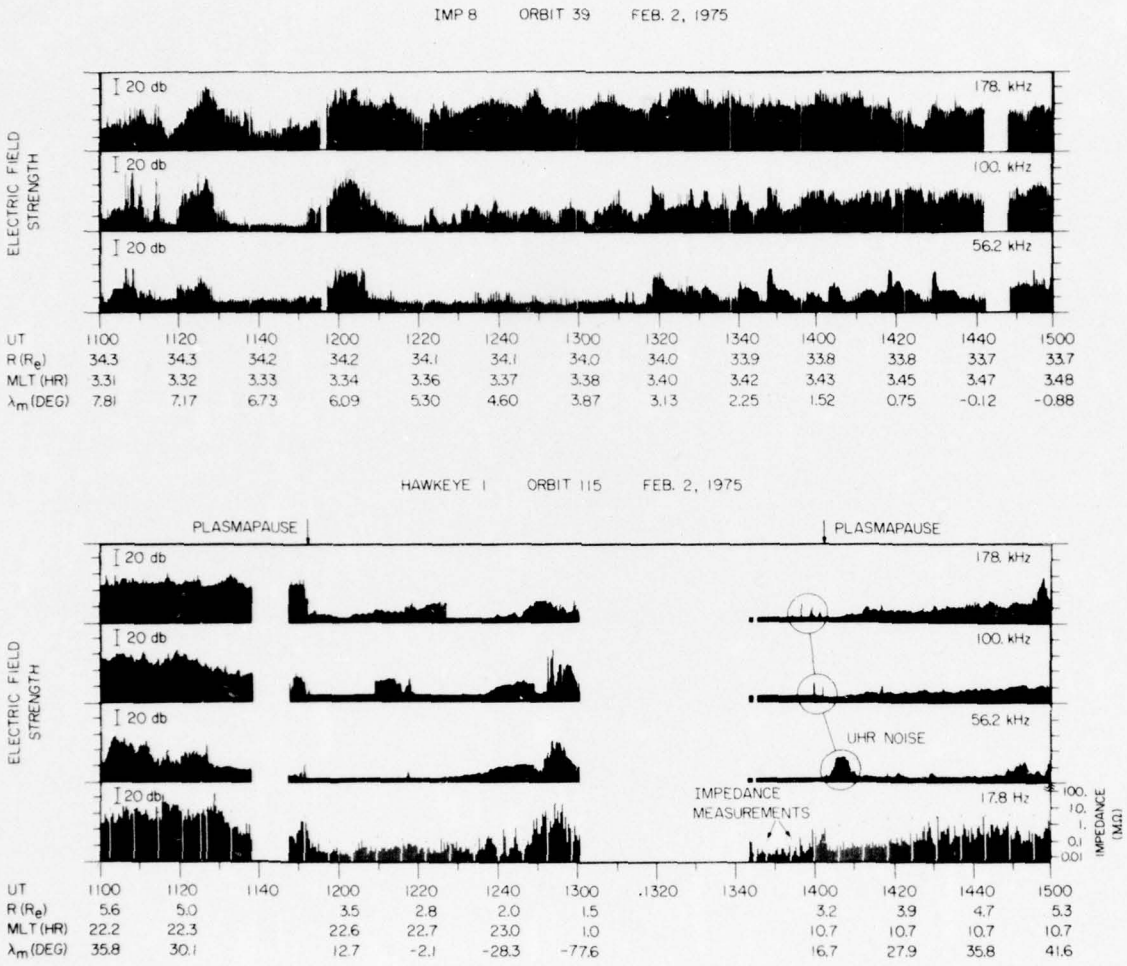
IMP 8 ORBIT 39 FEB. 2, 1975
ELECTRIC FIELD STRENGTH
20 db
178. kHz
100. kHz
56.2 kHz
UT 1100 1120 1140 1200 1220 1240 1300 1320 1340 1400 1420 1440 1500
R (Re) 34.3 34.3 34.2 34.2 34.1 34.1 34.0 34.0 33.9 33.8 33.8 33.7 33.7
MLT (HR) 3.31 3.32 3.33 3.34 3.36 3.37 3.38 3.40 3.42 3.43 3.45 3.47 3.48
λm (DEG) 7.81 7.17 6.73 6.09 5.30 4.60 3.87 3.13 2.25 1.52 0.75 -0.12 -0.88
HAWKEYE 1 ORBIT 115 FEB. 2, 1975
PLASMAPAUSE
PLASMAPAUSE
ELECTRIC FIELD STRENGTH
20 db
178. kHz
100. kHz
56.2 kHz
UHR NOISE
IMPEDANCE MEASUREMENTS
17.8 Hz
IMPEDANCE (MΩ)
100.
10.
1.
0.1
.001
UT 1100 1120 1140 1200 1220 1240 1300 1320 1340 1400 1420 1440 1500
R (Re) 5.6 5.0 3.5 2.8 2.0 1.5 3.2 3.9 4.7 5.3
MLT (HR) 22.2 22.3 22.6 22.7 23.0 1.0 10.7 10.7 10.7 10.7
λm (DEG) 35.8 30.1 12.7 -2.1 -28.3 -77.6 16.7 27.9 35.8 41.6

Figure 9

B-G76-90-1

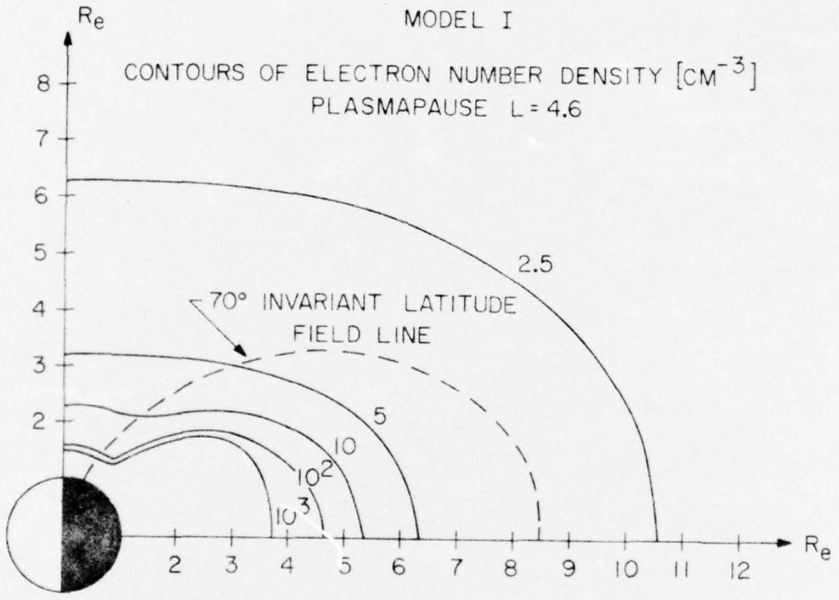

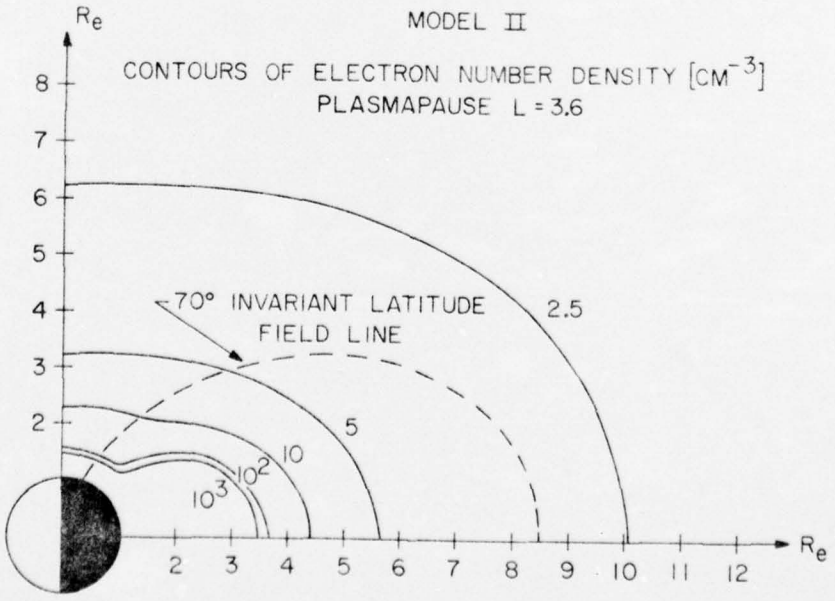

Figure 10

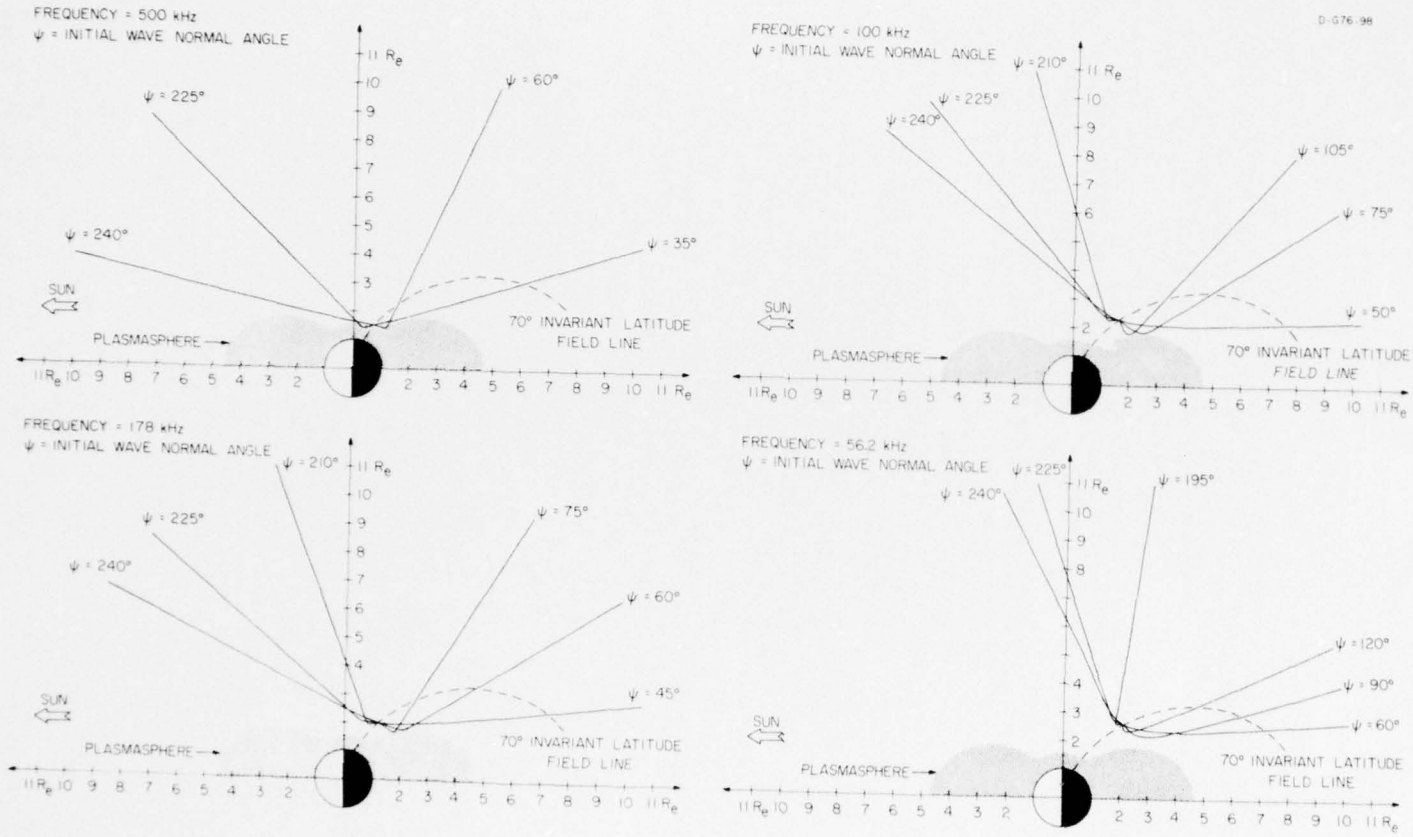
FREQUENCY = 500 kHz
ψ = INITIAL WAVE NORMAL ANGLE
ψ = 225°
ψ = 60°
ψ = 240°
ψ = 35°
SUN
PLASMASPHERE
70° INVARIANT LATITUDE FIELD LINE
11 Re 10 9 8 7 6 5 4 3 2
2 3 4 5 6 7 8 9 10 11 Re
FREQUENCY = 100 kHz
ψ = INITIAL WAVE NORMAL ANGLE
ψ = 210°
ψ = 225°
ψ = 240°
ψ = 105°
ψ = 75°
ψ = 50°
SUN
PLASMASPHERE
70° INVARIANT LATITUDE FIELD LINE
FREQUENCY = 178 kHz
ψ = INITIAL WAVE NORMAL ANGLE
ψ = 210°
ψ = 225°
ψ = 240°
ψ = 75°
ψ = 60°
ψ = 45°
SUN
PLASMASPHERE
70° INVARIANT LATITUDE FIELD LINE
FREQUENCY = 56.2 kHz
ψ = INITIAL WAVE NORMAL ANGLE
ψ = 225°
ψ = 240°
ψ = 195°
ψ = 120°
ψ = 90°
ψ = 60°
SUN
PLASMASPHERE
70° INVARIANT LATITUDE FIELD LINE

Figure 11

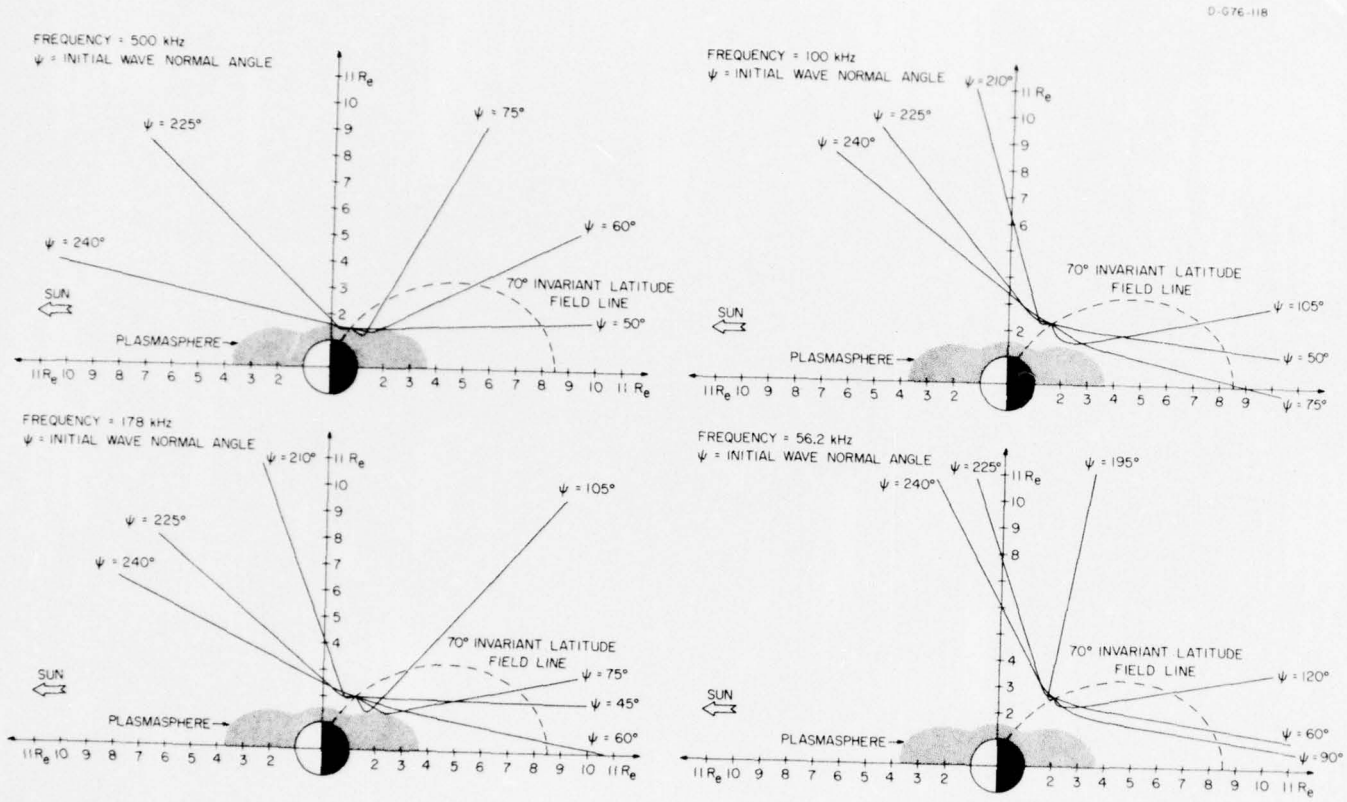
D-G76-118
FREQUENCY = 500 kHz
ψ = INITIAL WAVE NORMAL ANGLE
ψ = 225°
ψ = 75°
ψ = 240°
ψ = 60°
70° INVARIANT LATITUDE FIELD LINE
SUN
ψ = 50°
PLASMASPHERE
FREQUENCY = 100 kHz
ψ = INITIAL WAVE NORMAL ANGLE
ψ = 210°
ψ = 225°
ψ = 240°
70° INVARIANT LATITUDE FIELD LINE
ψ = 105°
SUN
ψ = 50°
PLASMASPHERE
ψ = 75°
FREQUENCY = 178 kHz
ψ = INITIAL WAVE NORMAL ANGLE
ψ = 210°
ψ = 105°
ψ = 225°
ψ = 240°
70° INVARIANT LATITUDE FIELD LINE
SUN
ψ = 75°
ψ = 45°
PLASMASPHERE
ψ = 60°
FREQUENCY = 56.2 kHz
ψ = INITIAL WAVE NORMAL ANGLE
ψ = 225°
ψ = 195°
ψ = 240°
70° INVARIANT LATITUDE FIELD LINE
ψ = 120°
SUN
ψ = 60°
PLASMASPHERE
ψ = 90°

Figure 12

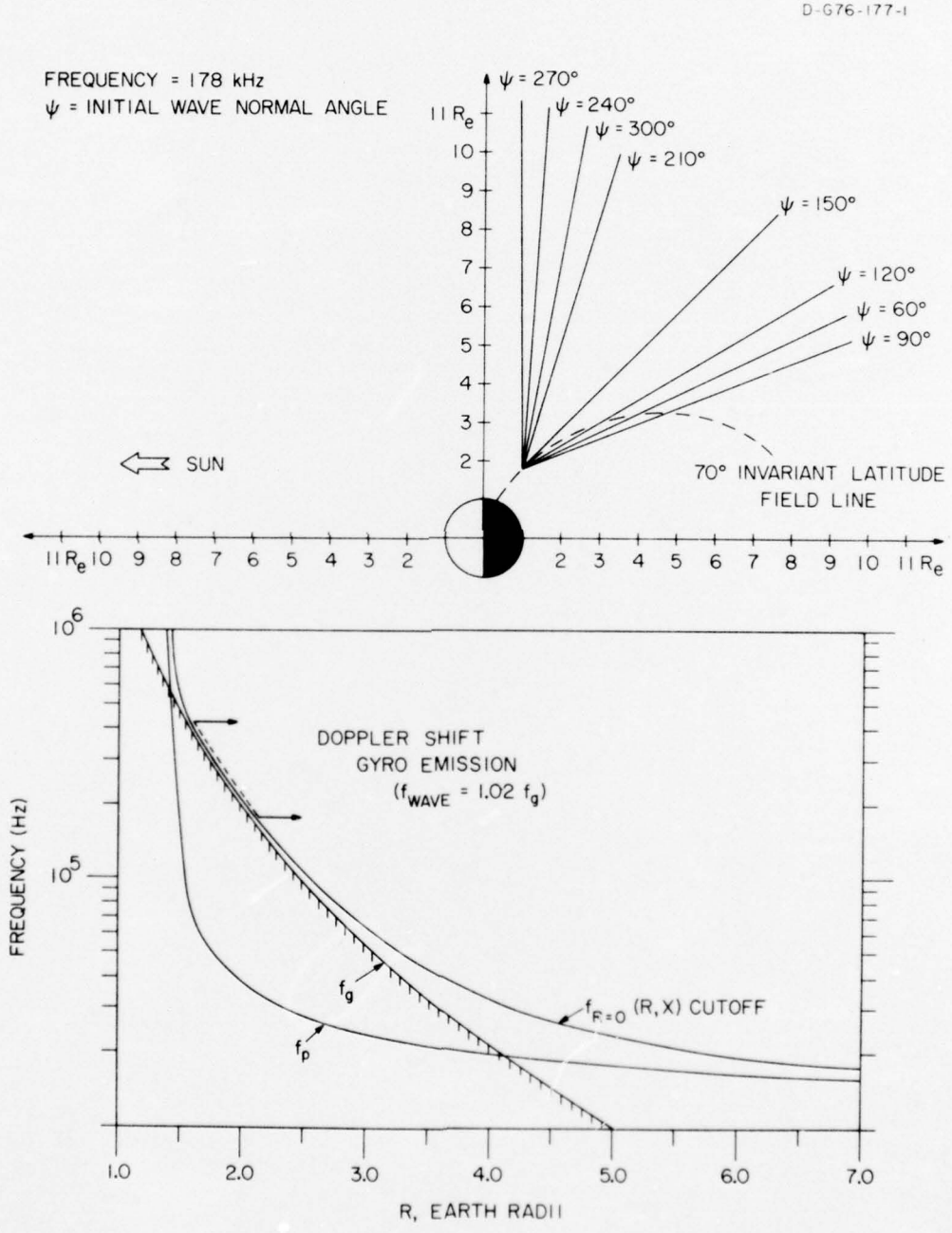
D-G76-177-1
FREQUENCY = 178 kHz
ψ = INITIAL WAVE NORMAL ANGLE
ψ = 270°
ψ = 240°
ψ = 300°
ψ = 210°
ψ = 150°
ψ = 120°
ψ = 60°
ψ = 90°
11 Re
10
9
8
7
6
5
4
3
2
SUN
70° INVARIANT LATITUDE
FIELD LINE
11Re 10 9 8 7 6 5 4 3 2
2 3 4 5 6 7 8 9 10 11Re
10^6
10^5
FREQUENCY (Hz)
DOPPLER SHIFT
GYRO EMISSION
(f_WAVE = 1.02 f_g)
f_g
f_p
f_R=0 (R,X) CUTOFF
1.0
2.0
3.0
4.0
5.0
6.0
7.0
R, EARTH RADII

Figure 13

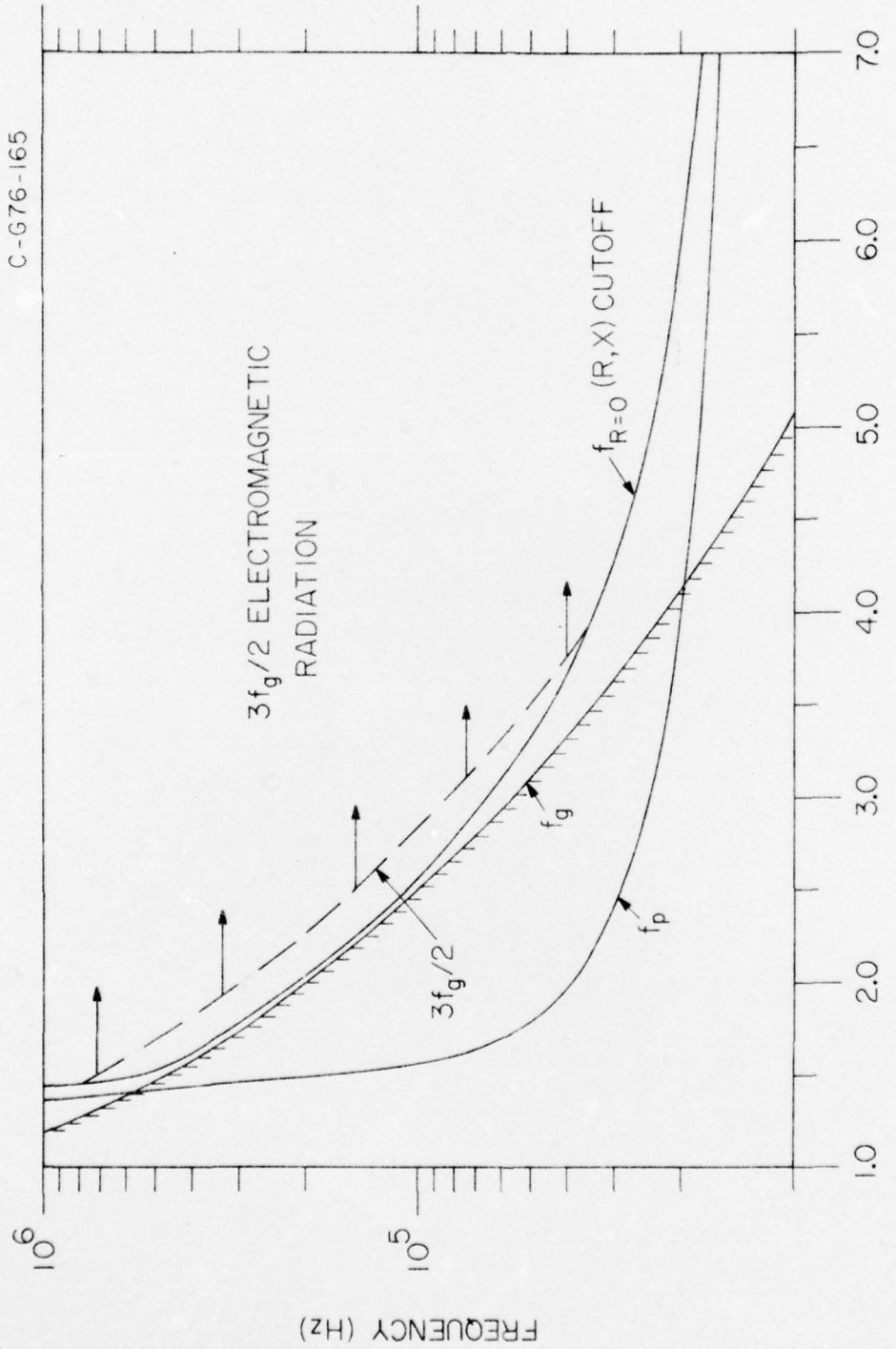
C-G76-165
$3f_g/2$ ELECTROMAGNETIC RADIATION
$f_{R=0}$ (R,X) CUTOFF
$3f_g/2$
f_g
f_p
FREQUENCY (Hz)
10^6
10^5
1.0
2.0
3.0
4.0
5.0
6.0
7.0
R, EARTH RADII

Figure 14

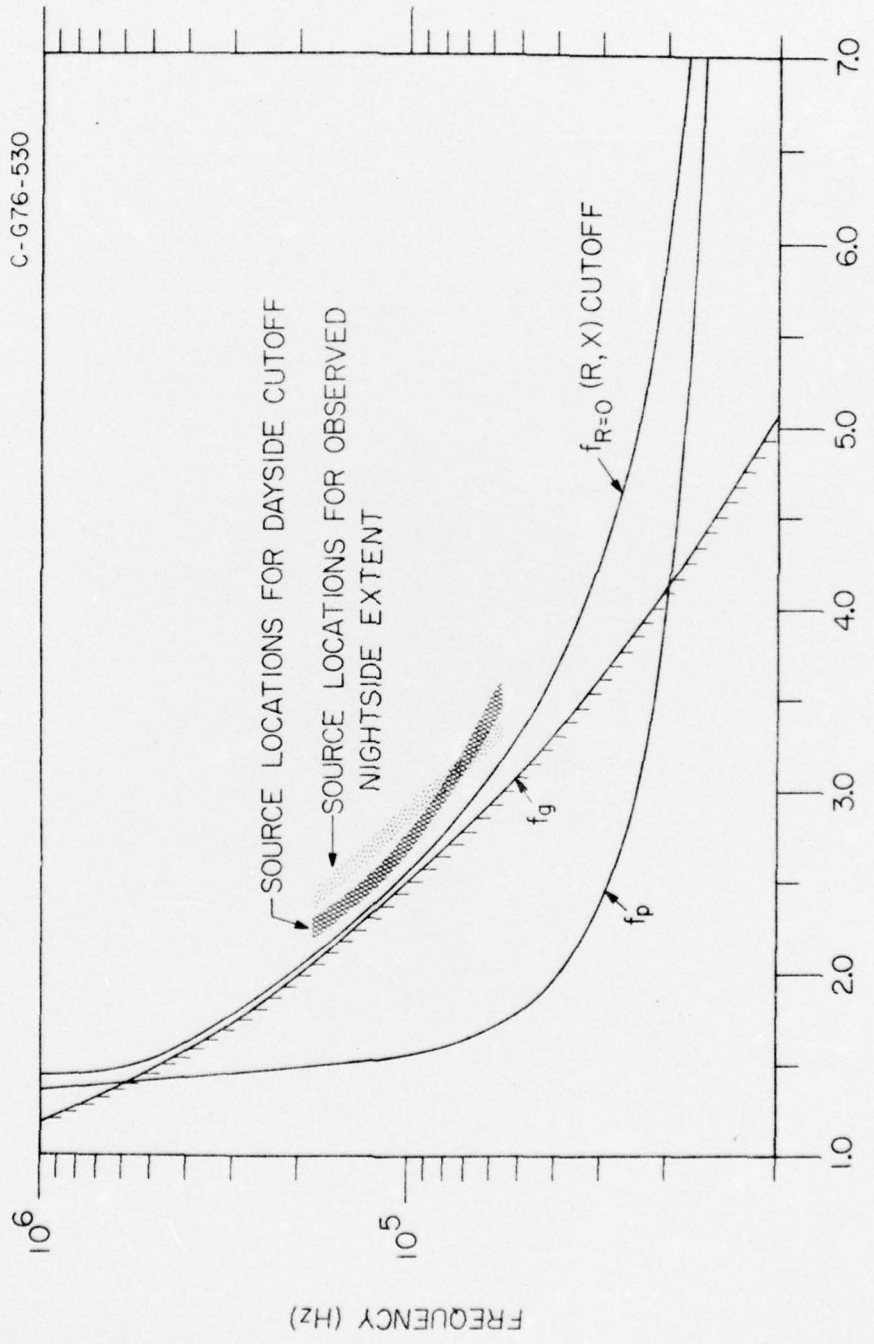
C-G76-530
SOURCE LOCATIONS FOR DAYSIDE CUTOFF
SOURCE LOCATIONS FOR OBSERVED NIGHTSIDE EXTENT
$f_{R=0}$ (R, X) CUTOFF
f_g
f_p
FREQUENCY (Hz)
10^6
10^5
1.0
2.0
3.0
4.0
5.0
6.0
7.0
R, EARTH RADII

Figure 15